

Energy Loss in Holographic Anisotropic Model for Heavy Quarks in External Magnetic Field

Irina Ya. Aref'eva^a, Kristina Rannu^a and Pavel Slepov^a

^a*Steklov Mathematical Institute, Russian Academy of Sciences,
Gubkina str. 8, 119991, Moscow, Russia*

E-mail: arefeva@mi-ras.ru, rannu-ka@rudn.ru, slepov@mi-ras.ru

ABSTRACT: Energy loss in anisotropic hot dense QGP in external magnetic field is studied within holographic approach. Energy loss is calculated by estimation of behaviour of the spatial Wilson loops using the effective potential technique. We examine the dependence of the effective potential on the spatial Wilson loops orientation in fully anisotropic background. For this purpose we obtain general formulas for the effective potential and study appearance of the effective potential dynamical wall. We consider particular fully anisotropic model [1] supported by Einstein-Dilaton-three-Maxwell action. The effective potential strongly depends on the parameters of anisotropy and magnetic field, therefore the energy loss depends on physical parameters – T , μ , c_B and orientation. Orientation is determined by angles between the moving heavy quark velocity, the axis of heavy ions collision and their impact parameter vector.

KEYWORDS: holography, AdS/QCD, energy loss, drag forces, spatial Wilson loops, phase transition, heavy quarks, magnetic field

Contents

1	Introduction	1
2	Setup. Spatial Wilson loops in fully anisotropic background	3
2.1	Arbitrary Orientation	3
2.2	Born-Infeld type action and large ℓ asymptotics	5
2.3	Particular cases and DW equations	7
2.4	Model and its thermodynamical properties	9
3	Numerical Results	14
3.1	Wilson loop W_{xY_1}	14
3.2	Wilson loop W_{xY_2}	18
3.3	Wilson loop $W_{y_1Y_2}$	24
4	Conclusion	26
5	Acknowledgments	27
A	EOM solution	28

1 Introduction

Nowadays holographic approach to study quark-gluon plasma (QGP) is actively developed [2–7] (and refs therein). Holography is one of the most effective tools to investigate the ultrarelativistic heavy-ion collisions (HIC). Different experimental data such as transport coefficients, thermalization time, multiplicity, direct-photon spectra etc. can be described within holographic QCD (HQCD). It is also expected that holography predicts more detailed form of QCD phase diagram. Different isotropic and anisotropic models holographic models to describe QGP were considered in [1–62].

One of HQCD models' classes is based on the Einstein-dilaton-Maxwell action, where the Maxwell field supports chemical potential. Choice of the warp factor in the metrics strongly influences the phase transition structure of HQCD. This choice should be done with correspondence to lattice results (Columbia plot) [63, 64].

It is important to add anisotropy into the holographic theory [17] as QGP is an anisotropic media just after the HIC. To deal with anisotropic HQCD one considers

Einstein-dilaton-two Maxwell model with additional Maxwell field to support the anisotropy in metrics. Such anisotropic model was considered in [39, 41] to reconstruct heavy quarks scenario and in [58] for the light quarks case. In these models anisotropy is defined by a parameter ν . The value $\nu = 4.5$ gives an accordance with the experimental data for the energy dependence of the total multiplicity of particles created in HIC. Isotropic holographic models had not been able to reproduce this experimental dependence ([22] and refs therein). The model [39] describes smeared confinement/deconfinement phase transitions, as the position of the confinement/deconfinement phase transition line depends on orientation of quark pair in respect to the HIC line [41]. That model also indicates the relations of the fluctuations of the multiplicity, i.e. the entanglement entropy, with the background phase transitions [53]. The anisotropy of the background metric also influences on corresponding jet quenching [17, 29, 38].

In this paper we calculated spatial Wilson loops (SWL) in a fully anisotropic holographic model for heavy quarks. It is known that for isotropic models the string tension of SWL is proportional to the corresponding drag force [65, 66]. This relation with a small modification takes place also for anisotropic models [7]. Therefore we can calculate SWL to estimate the drag forces for a quark moving in QGP. Drag forces defining energy loss are the subject of intensive studies in holographic approach [66–81]. In this paper the SWLs are calculated in the model set up by Einstein-dilaton-three-Maxwell action and describe two different types of anisotropy: anisotropy for producing the multiplicity dependence on energy and anisotropy associated with the magnetic field [1].

This paper is organised as follows. In Subsect.2.1 the Born-Infeld action for SWL in fully anisotropic background is presented. In Subsect.2.2 the large ℓ asymptotic of the Born-Infeld action for SWL are calculated. In Subsect.2.3 explicit forms of dynamical wall (DW) equations are defined and asymptotics for particular cases of orientations of SWL are presented. In Subsect.2.4 Einstein-dilaton-three-Maxwell holographic anisotropic model [1] and its thermodynamic properties are described. In Sect.3 SWL are considered in the metric supported by Einstein-dilaton-three-Maxwell action and effective potentials' dependence on magnetic field and HIC anisotropy are studied. The conclusion is given in Sect.4. Some formulas describing the model [1] are presented in Appendix A.

2 Setup. Spatial Wilson loops in fully anisotropic background

2.1 Arbitrary Orientation

We consider fully anisotropic background

$$ds^2 = G_{\mu\nu}dx^\mu dx^\nu = \frac{L^2 \mathfrak{b}(z)}{z^2} \left[-g(z)dt^2 + \mathfrak{g}_1 dx^2 + \mathfrak{g}_2 dy_1^2 + \mathfrak{g}_3 dy_2^2 + \frac{dz^2}{g(z)} \right] \quad (2.1)$$

and are going to calculate differently oriented SWLs in this background.

Following the holographic approach we have to calculate the value of the Nambu-Goto action for test string in the background (2.1):

$$S = \frac{1}{2\pi\alpha'} \int d\xi^1 d\xi^2 \sqrt{-\det h_{\alpha\beta}}, \quad (2.2)$$

where the induced metric

$$h_{\alpha\beta} = G_{\mu\nu} \partial_\alpha X^\mu \partial_\beta X^\nu. \quad (2.3)$$

depends on the orientation. Here we use the same parametrization of the orientation of Wilson rectangle as specified the entanglement rectangular parallelepiped in [53]. In 3-dimensional space the parameters specifying orientations of both objects, the rectangle in 3D space and rectangular parallelepiped, were the same. There is obvious difference in parametrizations of the world surface for the Wilson rectangle and world volume of rectangular parallelepiped.

To get the parametrization of the world sheet we use the representation of the rotation matrix $M(\phi, \theta, \psi)$ in 3-dimensional space

$$x^i = \sum_{j=1,2,3} a_{ij}(\phi, \theta, \psi) \zeta^j, \quad i = 1, 2, 3, \quad (2.4)$$

in terms of the Euler angles ϕ, θ, ψ :

$$M(\phi, \theta, \psi) = \begin{pmatrix} a_{11}(\phi, \theta, \psi) & a_{12}(\phi, \theta, \psi) & a_{13}(\phi, \theta, \psi) \\ a_{21}(\phi, \theta, \psi) & a_{22}(\phi, \theta, \psi) & a_{23}(\phi, \theta, \psi) \\ a_{31}(\phi, \theta, \psi) & a_{32}(\phi, \theta, \psi) & a_{33}(\phi, \theta, \psi) \end{pmatrix} \quad (2.5)$$

where

$$\begin{aligned} a_{11}(\phi, \theta, \psi) &= \cos \phi \cos \psi - \cos \theta \sin \phi \sin \psi, \\ a_{12}(\phi, \theta, \psi) &= -\cos \psi \sin \phi - \cos \phi \cos \theta \sin \psi, \\ a_{13}(\phi, \theta, \psi) &= \sin \theta \sin \psi, \\ a_{21}(\phi, \theta, \psi) &= \cos \theta \cos \psi \sin \phi + \cos \phi \sin \psi, \\ a_{22}(\phi, \theta, \psi) &= \cos \phi \cos \theta \cos \psi - \sin \phi \sin \psi, \\ a_{23}(\phi, \theta, \psi) &= -\cos \psi \sin \theta, \\ a_{31}(\phi, \theta, \psi) &= \sin \phi \sin \theta, \\ a_{32}(\phi, \theta, \psi) &= \cos \phi \sin \theta, \\ a_{33}(\phi, \theta, \psi) &= \cos \theta. \end{aligned} \quad (2.6)$$

Here ϕ is the angle between ζ^1 -axis and the node line (N), θ is the angle between ζ^3 and x^3 -axes, ψ is the angle between the node line N and x^1 -axis.

To describe the nesting of the 2-dimensional world sheet in 5-dimensional space time we use

$$\begin{aligned} X^0(\xi) &= \text{const}, \\ X^i(\xi) &= \sum_{\alpha=1,2} a_{i\alpha}(\phi, \theta, \psi) \xi^\alpha, \quad i = 1, 2, 3, \quad \alpha = 1, 2, \\ X^4(\xi) &= z(\xi^1), \end{aligned} \quad (2.7)$$

where x^i are spatial coordinates and $a_{ij}(\phi, \theta, \psi)$ are entries of the rotation matrix.

We write the line element of the induced metric for the arbitrary oriented spatial Wilson loop as

$$ds^2 = g_{\alpha\beta} d\xi^\alpha d\xi^\beta, \quad \alpha, \beta = 1, 2 \quad (2.8)$$

and substitute the differentials dx^M following from the embedding relations (2.7):

$$\begin{aligned} ds^2 &= \frac{L^2 b_s(z)}{z^2} \left(\sum_{i=1,2,3} \mathfrak{g}_i(z) d(x^i)^2 + \frac{d(x^4)^2}{g} \right) \\ &= \frac{L^2 b_s(z)}{z^2} \left(\sum_{i=1,2,3} \mathfrak{g}_i(z) \left(\sum_{j=1,2} a_{ij}(\phi, \theta, \psi) d\xi^j \right)^2 + z'^2 \frac{d(\xi^1)^2}{g(z)} \right). \end{aligned} \quad (2.9)$$

We have

$$\begin{aligned} g_{\alpha\beta} &= \frac{L^2 b_s(z)}{z^2} \bar{g}_{\alpha\beta}, \\ \bar{g}_{11}(z, \phi, \theta, \psi) &= \mathfrak{g}_1 a_{11}^2 + \mathfrak{g}_2 a_{21}^2 + \mathfrak{g}_3 a_{31}^2 + \frac{z'^2}{g}, \\ \bar{g}_{22}(z, \phi, \theta, \psi) &= \mathfrak{g}_1 a_{12}^2 + \mathfrak{g}_2 a_{22}^2 + \mathfrak{g}_3 a_{32}^2, \\ \bar{g}_{12}(z, \phi, \theta, \psi) &= \mathfrak{g}_1 a_{11} a_{12} + \mathfrak{g}_2 a_{21} a_{22} + \mathfrak{g}_3 a_{13} a_{32}, \\ \bar{g}_{21} &= \bar{g}_{12}. \end{aligned} \quad (2.11)$$

Determinant of the induced metric for SWL is

$$\begin{aligned} \det g_{\alpha\beta} &= \left(\frac{L^2 b_s}{z^2} \right)^2 \left(\left(\mathfrak{g}_1 a_{11}^2 + \mathfrak{g}_2 a_{21}^2 + \mathfrak{g}_3 a_{31}^2 + \frac{z'^2}{g} \right) (\mathfrak{g}_1 a_{12}^2 + \mathfrak{g}_2 a_{22}^2 + \mathfrak{g}_3 a_{32}^2) - \right. \\ &\quad \left. - (\mathfrak{g}_1 a_{11} a_{12} + \mathfrak{g}_2 a_{21} a_{22} + \mathfrak{g}_3 a_{13} a_{32})^2 \right). \end{aligned} \quad (2.12)$$

The Nambu-Goto action for SWL is given by integration over the world sheet \mathcal{W}

$$\mathcal{S}_{SWL} = \int_{\mathcal{W}} \left(\frac{L^2 b_s}{z^2} \right) \sqrt{\left(\mathfrak{g}_1 \mathfrak{g}_2 a_{33}^2 + \mathfrak{g}_1 \mathfrak{g}_3 a_{23}^2 + \mathfrak{g}_2 \mathfrak{g}_3 a_{13}^2 + \mathfrak{g}_3^2 a_{32}^2 (a_{31}^2 - a_{13}^2) + \frac{z'^2}{g} \bar{g}_{22} \right)} d\xi^1 d\xi^2. \quad (2.13)$$

The effective potential is

$$\mathcal{V}(z(\xi)) = \left(\frac{L^2 b_s}{z^2} \right) \sqrt{\mathfrak{g}_1 \mathfrak{g}_2 a_{33}^2 + \mathfrak{g}_1 \mathfrak{g}_3 a_{23}^2 + \mathfrak{g}_2 \mathfrak{g}_3 a_{13}^2 + \mathfrak{g}_3^2 a_{32}^2 (a_{31}^2 - a_{13}^2)}. \quad (2.14)$$

The effective potential and the action depend on the angles and anisotropy. This result can be compared with the action and the effective potential for holographic entanglement entropy (HEE) [53]:

$$\mathcal{S}_{HEE} = \int_{\mathcal{P}} \left(\frac{L^2 b_s}{z^2} \right)^{3/2} \sqrt{\left(\mathfrak{g}_1 \mathfrak{g}_2 \mathfrak{g}_3 + \frac{z'^2}{g} (\bar{g}_{22} \bar{g}_{33} - \bar{g}_{23}^2) \right)} d\xi^1 d\xi^2 d\xi^3, \quad (2.15)$$

$$\mathcal{V}_{HEE}(z) = \left(\frac{L^2 b_s}{z^2} \right)^{3/2} \sqrt{\mathfrak{g}_1 \mathfrak{g}_2 \mathfrak{g}_3}, \quad (2.16)$$

where $g, \mathfrak{g}_1, \mathfrak{g}_2, \mathfrak{g}_3$ are functions of z and $\bar{g}_{22}, \bar{g}_{33}, \bar{g}_{23}$ are functions of z and the Euler angles. Note that the effective potential for HEE does not depend on the angles.

2.2 Born-Infeld type action and large ℓ asymptotics

The considered actions for SWL, temporal WL and HEE [6, 49, 53] are the particular cases of the BI action:

$$\mathcal{S} = \int_{-\ell/2}^{\ell/2} M(z(\xi)) \sqrt{\mathcal{F}(z(\xi)) + (z'(\xi))^2} d\xi. \quad (2.17)$$

This action defines the dynamical system with a dynamic variable $z = z(\xi)$ and time ξ . The effective potential is

$$\mathcal{V}(z(\xi)) \equiv M(z(\xi)) \sqrt{\mathcal{F}(z(\xi))}. \quad (2.18)$$

This system has the first integral:

$$\frac{M(z(\xi)) \mathcal{F}(z(\xi))}{\sqrt{\mathcal{F}(z(\xi)) + (z'(\xi))^2}} = \mathcal{I}. \quad (2.19)$$

From (2.19) we can find the “top” point z_* (the closed position of the minimal surface to the horizon), where $z'(\xi) = 0$:

$$M(z_*) \sqrt{\mathcal{F}(z_*)} = \mathcal{I}. \quad (2.20)$$

Finding z' from (2.19) one gets representations for the length ℓ and the action \mathcal{S} (2.17):

$$\frac{\ell}{2} = \int_0^{z_*} \frac{1}{\sqrt{\mathcal{F}(z)}} \frac{dz}{\sqrt{\frac{\mathcal{V}^2(z)}{\mathcal{V}^2(z_*)} - 1}}, \quad (2.21)$$

$$\frac{\mathcal{S}}{2} = \int_{\epsilon}^{z_*} \frac{M(z) dz}{\sqrt{1 - \frac{\mathcal{V}^2(z_*)}{\mathcal{V}^2(z)}}}. \quad (2.22)$$

We have two options to have $\ell \rightarrow \infty$.

- The existence of a stationary point of $\mathcal{V}(z)$

$$\mathcal{V}' \Big|_{z_{DW}} = 0. \quad (2.23)$$

This point is called a dynamical wall (DW) point. One takes the top point z_* equal to the dynamical wall position. Since near the top point

$$\sqrt{\frac{\mathcal{V}^2(z)}{\mathcal{V}^2(z_{DW})}} - 1 = \sqrt{\frac{\mathcal{V}''(z_{DW})}{\mathcal{V}(z_{DW})}}(z - z_*) + \mathcal{O}((z - z_*)^2), \quad (2.24)$$

one gets

$$\ell \underset{z \rightarrow z_*}{\sim} \frac{1}{\sqrt{F(z_{DW})}} \sqrt{\frac{\mathcal{V}(z_{DW})}{\mathcal{V}''(z_{DW})}} \log(z - z_*), \quad (2.25)$$

$$\mathcal{S} \underset{z \rightarrow z_*}{\sim} M(z_{DW}) \sqrt{\frac{\mathcal{V}(z_{DW})}{\mathcal{V}''(z_{DW})}} \log(z - z_*). \quad (2.26)$$

Hence

$$\mathcal{S} \sim M(z_{DW}) \cdot \sqrt{F(z_{DW})} \cdot \ell, \quad (2.27)$$

$$\sigma_{DW} = M(z_{DW}) \sqrt{F(z_{DW})}. \quad (2.28)$$

- There is no stationary point of $\mathcal{V}(z)$ in the region $0 < z < z_h$, and we suppose it to be near horizon

$$F(z) = \mathfrak{F}(z_h)(z_h - z) + \mathcal{O}((z_h - z)^2), \quad (2.29)$$

i.e. near horizon (the sting stretch on the horizon). In this case we take $z_* = z_h$ and there are the following options:

- if $M(z_h) \neq \infty$, we have

$$\ell \rightarrow \infty, \quad (2.30)$$

$$\mathcal{S} \rightarrow 0; \quad (2.31)$$

- if $M(z) \xrightarrow{z \rightarrow z_h} \infty$ as

$$M(z) \underset{z \sim z_h}{\sim} \frac{\mathfrak{m}(z_h)}{\sqrt{z - z_h}}, \quad (2.32)$$

we have

$$\ell \underset{z \rightarrow z_h}{\sim} \frac{1}{\sqrt{\mathfrak{F}(z_h)}} \frac{1}{\sqrt{-\frac{2\mathcal{V}'(z_h)}{\mathcal{V}(z_h)}}} \log(z - z_h), \quad (2.33)$$

$$\mathcal{S} \underset{z \rightarrow z_*}{\sim} \mathfrak{m}(z_h) \frac{1}{\sqrt{-\frac{2\mathcal{V}'(z_h)}{\mathcal{V}(z_h)}}} \log(z - z_h) \quad (2.34)$$

and therefore

$$\sigma_h = \mathfrak{m}(z_h) \mathfrak{F}^{1/2}(z_h). \quad (2.35)$$

2.3 Particular cases and DW equations

Let us consider particular cases of (2.14) and (2.13) to understand the picture with SWLs in fully anisotropic background more instructively.

1) $\phi = 0, \theta = 0, \psi = 0$; $a_{11} = a_{22} = a_{33} = 1, a_{12} = a_{21} = a_{31} = a_{31} = a_{32} = a_{23} = 0$:

$$\mathcal{S}_{xY_1} = \int_{\mathcal{P}} \left(\frac{L^2 b_s}{z^2} \right) \sqrt{\left(\mathfrak{g}_1 \mathfrak{g}_2 + \frac{z'^2}{g} \mathfrak{g}_2 \right)} d\xi^1 d\xi^2, \quad (2.36)$$

$$\mathcal{V}_{xY_1}(z(\xi)) = \left(\frac{L^2 b_s}{z^2} \right) \sqrt{\mathfrak{g}_1 \mathfrak{g}_2}; \quad (2.37)$$

2) $\phi = \pi/2, \theta = 0, \psi = 0$; $a_{21} = a_{33} = -a_{12} = 1, a_{11} = a_{13} = a_{22} = a_{23} = a_{31} = a_{32} = 0$:

$$\mathcal{S}_{Xy_1} = \int_{\mathcal{P}} \left(\frac{L^2 b_s}{z^2} \right) \sqrt{\left(\mathfrak{g}_1 \mathfrak{g}_2 + \frac{z'^2}{g} \mathfrak{g}_1 \right)} d\xi^1 d\xi^2, \quad (2.38)$$

$$\mathcal{V}_{Xy_1}(z(\xi)) = \left(\frac{L^2 b_s}{z^2} \right) \sqrt{\mathfrak{g}_1 \mathfrak{g}_2}; \quad (2.39)$$

3) $\phi = 0, \theta = \pi/2, \psi = 0$; $a_{11} = -a_{23} = a_{32} = 1, a_{12} = a_{13} = a_{21} = a_{22} = a_{31} = a_{33} = 0$:

$$\mathcal{S}_{xY_2} = \int_{\mathcal{P}} \left(\frac{L^2 b_s}{z^2} \right) \sqrt{\left(\mathfrak{g}_1 \mathfrak{g}_3 + \frac{z'^2}{g} \mathfrak{g}_3 \right)} d\xi^1 d\xi^2, \quad (2.40)$$

$$\mathcal{V}_{xY_2}(z(\xi)) = \left(\frac{L^2 b_s}{z^2} \right) \sqrt{\mathfrak{g}_1 \mathfrak{g}_3}; \quad (2.41)$$

4) $\phi = \pi/2, \theta = \pi/2, \psi = -\pi/2$; $a_{22} = a_{31} = -a_{13} = 1, a_{11} = a_{12} = a_{21} = a_{23} = a_{32} = a_{33} = 0$:

$$\mathcal{S}_{y_1Y_2} = \int_{\mathcal{P}} \left(\frac{L^2 b_s}{z^2} \right) \sqrt{\left(\mathfrak{g}_2 \mathfrak{g}_3 + \frac{z'^2}{g} \mathfrak{g}_2 \right)} d\xi^1 d\xi^2, \quad (2.42)$$

$$\mathcal{V}_{y_1Y_2}(z(\xi)) = \left(\frac{L^2 b_s}{z^2} \right) \sqrt{\mathfrak{g}_2 \mathfrak{g}_3}. \quad (2.43)$$

These results correspond to [7]. The general form of the DW equation (if DW exists): $\mathcal{V}'(z) = 0$ [5, 8].

The equations for the DW for SWL in particular cases for different potentials:

$$\mathcal{DW}_{xY_1} = \mathcal{DW}_{Xy_1} \equiv \frac{2b'_s(z)}{b_s(z)} + \frac{\mathfrak{g}'_1(z)}{\mathfrak{g}_1(z)} + \frac{\mathfrak{g}'_2(z)}{\mathfrak{g}_2(z)} - \frac{4}{z} \Bigg|_{z=z_{DW}} = 0, \quad (2.44)$$

$$\mathcal{DW}_{xY_2} \equiv \frac{2b'_s(z)}{b_s(z)} + \frac{\mathfrak{g}'_1(z)}{\mathfrak{g}_1(z)} + \frac{\mathfrak{g}'_3(z)}{\mathfrak{g}_3(z)} - \frac{4}{z} \Bigg|_{z=z_{DW}} = 0, \quad (2.45)$$

$$\mathcal{DW}_{y_1Y_2} \equiv \frac{2b'_s(z)}{b_s(z)} + \frac{\mathfrak{g}'_2(z)}{\mathfrak{g}_2(z)} + \frac{\mathfrak{g}'_3(z)}{\mathfrak{g}_3(z)} - \frac{4}{z} \Bigg|_{z=z_{DW}} = 0. \quad (2.46)$$

Let us take the metric in the string frame that supported by Einstein-dilaton-three Maxwell action that was obtained in [1]:

$$ds^2 = \frac{L^2 b_s(z)}{z^2} \left[-g(z)dt^2 + dx^2 + \left(\frac{z}{L}\right)^{2-\frac{2}{\nu}} dy_1^2 + e^{c_B z^2} \left(\frac{z}{L}\right)^{2-\frac{2}{\nu}} dy_2^2 + \frac{dz^2}{g(z)} \right], \quad (2.47)$$

$$b_s(z) = e^{2\mathcal{A}(z) + \sqrt{\frac{2}{3}}\phi(z, z_0)}, \quad (2.48)$$

where L is the AdS-radius, $b_s(z)$ is the warp-factor, $\phi(z, z_0)$ is the dilaton field, z_0 is the point at which $\phi(z_0) = 0$ (the boundary condition for dilaton field), $g(z)$ is the blackening function, ν is the parameter of HIC anisotropy and c_B is the coefficient of secondary anisotropy related to the external magnetic field $F_{\mu\nu}^{(B)}$. Note that choice of $\mathcal{A}(z)$ determines the heavy/light quarks description of the model, so we follow previous works and consider $\mathcal{A}(z) = -cz^2/4$ for heavy quarks [39] and $\mathcal{A}(z) = -a \ln(bz^2 + 1)$ for light quarks [58]. Therefore for the solution [1] we can get $\mathfrak{g}_1 = 1$, $\mathfrak{g}_2 = (z/L)^{2-2/\nu}$, $\mathfrak{g}_3 = (z/L)^{2-2/\nu} e^{c_B z^2}$. For this particular case:

$$\sigma_{xY_1} = \sigma_{Xy_1} = \left(\frac{L^2 b_s(z)}{z^2}\right) \sqrt{\mathfrak{g}_1 \mathfrak{g}_2} = \left(\frac{L^{1+1/\nu} b_s(z)}{z^{1+1/\nu}}\right), \quad (2.49)$$

$$\sigma_{xY_2} = \left(\frac{L^2 b_s(z)}{z^2}\right) \sqrt{\mathfrak{g}_1 \mathfrak{g}_3} = \left(\frac{L^{1+1/\nu} b_s(z)}{z^{1+1/\nu}}\right) e^{c_B z^2/2}, \quad (2.50)$$

$$\sigma_{y_1Y_2} = \left(\frac{L^2 b_s(z)}{z^2}\right) \sqrt{\mathfrak{g}_2 \mathfrak{g}_3} = \left(\frac{L^{2/\nu} b_s(z)}{z^{2/\nu}}\right) e^{c_B z^2/2}, \quad (2.51)$$

where $z = z_h$ or $z = z_{DW}$ (if the dynamical wall exists).

Note that drag forces for metric (2.1) with $\mathfrak{g}_1 = 1$ have been calculated directly in [7] with the result

$$p_x = v_x \frac{b_s(z)}{z^2} \quad (2.52)$$

$$p_{y_1} = v_{y_1} \frac{b_s(z)}{z^2} \mathfrak{g}_2(z) \quad (2.53)$$

$$p_{y_2} = v_{y_2} \frac{b_s(z)}{z^2} \mathfrak{g}_3(z), \quad (2.54)$$

that reproduce (2.49), (2.50) and (2.51) for $\mathbf{g}_1 = 1$ if we identify

$$v_x = v \sqrt{\mathbf{g}_2}, \quad (2.55)$$

$$v_{y_1} = v \frac{\sqrt{\mathbf{g}_3}}{\mathbf{g}_2}, \quad (2.56)$$

$$v_{y_2} = v \frac{\sqrt{\mathbf{g}_2}}{\sqrt{\mathbf{g}_3}} \quad (2.57)$$

with some constant v .

2.4 Model and its thermodynamical properties

In the next sections we calculate the string tensions (2.49)-(2.51) and their dependence on the thermodynamic parameters and magnetic field. Most of the quantities we dealt with in the previous sections depend explicitly on z_h , while we need the temperature dependence. As we deal with the model considered in [1], we remind here its main features and specifically the behavior of temperature as function of z_h , c_B and μ .

We take the action in Einstein frame and the metric ansatz

$$S = \frac{1}{16\pi G_5} \int d^5x \sqrt{-g} \times \left[R - \frac{f_1(\phi)}{4} F^{(1)2} - \frac{f_2(\phi)}{4} F^{(2)2} - \frac{f_B(\phi)}{4} F^{(B)2} - \frac{1}{2} \partial_\mu \phi \partial^\mu \phi - V(\phi) \right], \quad (2.58)$$

$$\begin{aligned} F_{\mu\nu}^{(1)} &= \partial_\mu A_\nu - \partial_\nu A_\mu, \text{ i.e. } A_\mu^{(1)} = A_t(z) \delta_\mu^0, \\ F_{\mu\nu}^{(2)} &= q \, dy^1 \wedge dy^2, \text{ i.e. } F_{y_1 y_2}^{(2)} = q, \\ F_{\mu\nu}^{(B)} &= q_B \, dx \wedge dy^1, \text{ i.e. } F_{xy_1}^{(B)} = q_B, \end{aligned} \quad (2.59)$$

$$ds^2 = \frac{L^2}{z^2} \mathbf{b}(z) \left[-g(z) dt^2 + dx^2 + \left(\frac{z}{L} \right)^{2-\frac{2}{\nu}} dy_1^2 + e^{c_B z^2} \left(\frac{z}{L} \right)^{2-\frac{2}{\nu}} dy_2^2 + \frac{dz^2}{g(z)} \right], \quad (2.60)$$

$$\mathbf{b}(z) = e^{2\mathcal{A}(z)}, \quad (2.61)$$

where $\phi = \phi(z)$ is the scalar field, $f_1(\phi)$, $f_2(\phi)$ and $f_B(\phi)$ are the coupling functions associated with the Maxwell fields A_μ , $F_{\mu\nu}^{(2)}$ and $F_{\mu\nu}^{(B)}$ correspondingly, q and q_B are constants and $V(\phi)$ is the scalar field potential, L is the AdS-radius, $\mathbf{b}(z)$ is the warp factor in Einstein frame and $\mathcal{A}(z)$ is related with $\mathbf{b}(z)$ according (2.61), $g(z)$ is the blackening function, ν is the parameter of primary anisotropy, caused by non-symmetry of heavy-ion collision (HIC), and c_B is the coefficient of secondary anisotropy related to the external magnetic field $F_{\mu\nu}^{(B)}$. Choice of $\mathcal{A}(z)$ determines the heavy/light quarks description of the model, so we follow previous works and consider $\mathcal{A}(z) = -cz^2/4$ and $f_1 = z^{-2+\frac{2}{\nu}}$ for heavy quarks [39]. The EOM solution can be found in Appendix A.

Temperature and entropy can be written as:

$$T = \frac{|g'|}{4\pi} \Big|_{z=z_h} = \frac{1}{2\pi} \left| - e^{\frac{1}{4}(3c-2c_B)z_h^2} (2c_B - c) z_h^{1+\frac{2}{\nu}} \left\{ \frac{\mu^2 e^{\frac{1}{4}(c-2c_B)z_h^2}}{4L^2 \left(1 - e^{\frac{1}{4}(c-2c_B)z_h^2}\right)^2} + \right. \right. \\ \left. \left. + \left(\frac{3}{4}\right)^{1+\frac{1}{\nu}} \frac{(2c_B - c)^{\frac{1}{\nu}}}{\Gamma\left(1 + \frac{1}{\nu}; 0\right) - \Gamma\left(1 + \frac{1}{\nu}; \frac{3}{4}(2c_B - c)z_h^2\right)} \times \right. \right. \\ \left. \left. \times \left[1 - \frac{\mu^2 (2c_B - c)^{-\frac{1}{\nu}}}{4L^2 \left(1 - e^{\frac{1}{4}(c-2c_B)z_h^2}\right)^2} \left(\Gamma\left(1 + \frac{1}{\nu}; 0\right) - \Gamma\left(1 + \frac{1}{\nu}; (2c_B - c)z_h^2\right) \right) \right] \right\} \right|, \quad (2.62)$$

$$s = \frac{1}{4} \left(\frac{L}{z_h} \right)^{1+\frac{2}{\nu}} e^{-\frac{1}{4}(3c-2c_B)z_h^2}. \quad (2.63)$$

For zero chemical potential and zero magnetic field in holographic models describing heavy quarks behavior [39, 41] temperature is a two-valued function of horizon having a local minimum (Fig.1, 2). Increasing branch with larger z_h values is unstable, so the phase transition (collapse) to the decreasing (stable) branch with smaller z_h values along any isotherm $T > T_{min}$ is possible. Because of the local minimum temperatures $0 \leq T < T_{min}$ can't be reached thus limiting the possibility of the system cool-down.

Turning magnetic field or chemical potential on makes temperature a three-valued function due to a local maximum appearance (Fig.1A,B). Thus magnetic field and chemical potential reinforce each other's effect on the temperature behavior. Here the BH collapse and therefore the 1-st order phase transition are possible for $T_{min} < T < T_{max}$ where $T(z_h)$ is three-valued. Both decreasing branch with larger z_h (right) and increasing branch (middle) are unstable, and the collapse occurs from decreasing unstable branch to the decreasing stable one (left) bypassing through the increasing unstable interval between the local minimum and the local maximum. For $T > T_{max}$ and $0 \leq T < T_{min}$ phase transition doesn't happen but any temperatures are available.

As chemical potential and magnetic field have similar effect on the temperature there are rather narrow intervals of μ and c_B for which collapse is still possible. As we can see on plots of Fig.1A, even for $c_B = -0.015$ or $\mu = 0.1$ temperature is monotonic already. So the BH collapse and the 1-st order phase transition corresponding to it become very fragile in the magnetic field, and non-zero chemical potential only exacerbates this situation.

The other factor that becomes significant is the primary spatial anisotropy parametrized by the coefficient ν . It makes temperature extremes more pronounced and inhibits their smoothing longer (Fig.1C). This tendency keeps for non-zero μ

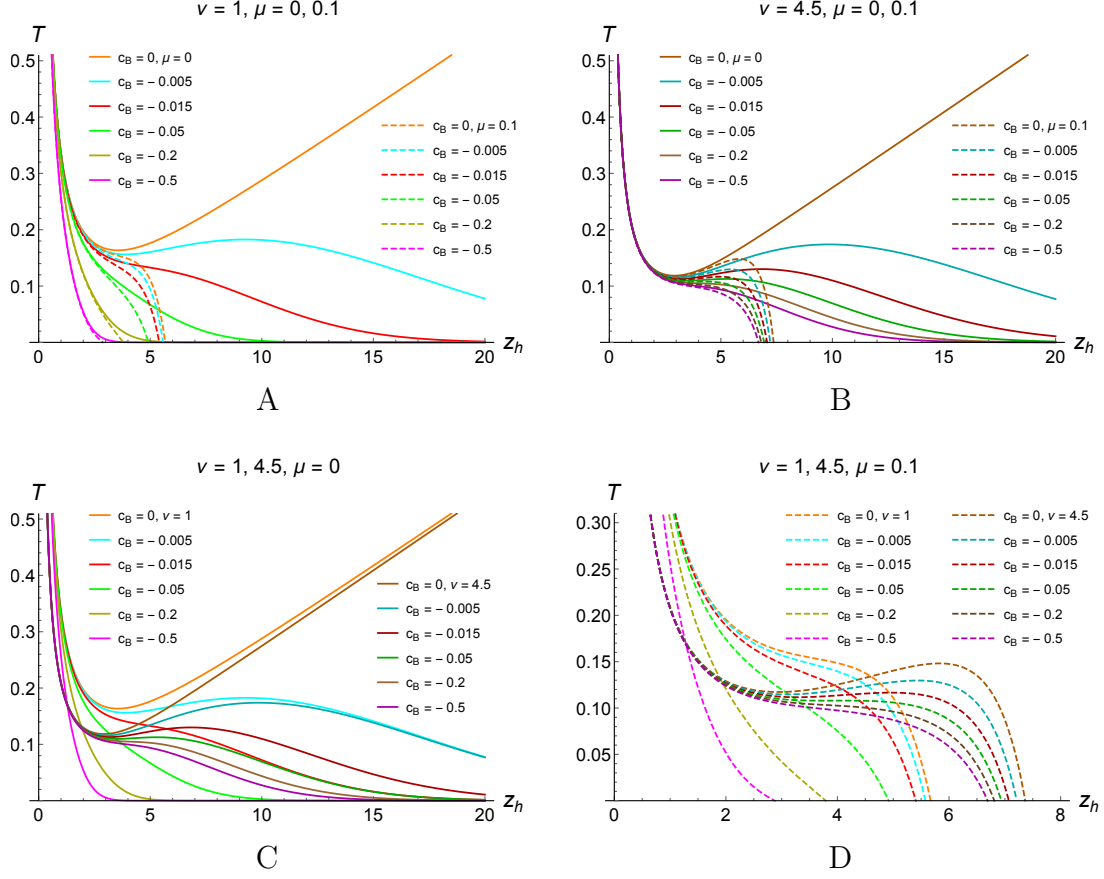


Figure 1. Temperature dependence on z_h for different c_B , $\mu = 0, 0.1$, $\nu = 1$ (A) and $\nu = 4.5$ (B); for $\nu = 1, 4.5$, $\mu = 0$ (C) and $\mu = 0.1$ (D).

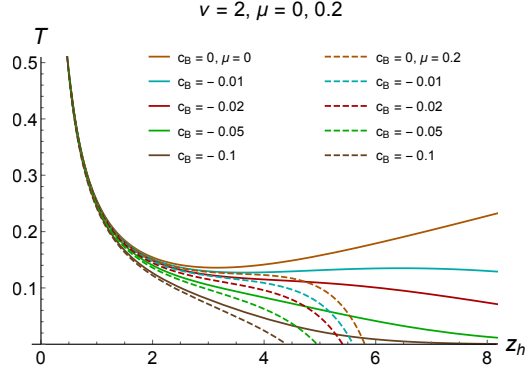


Figure 2. Temperature dependence on z_h for different c_B , $\nu = 2$, $\mu = 0, 0.2$.

(Fig.1D), thus making phase transition more resistant to stronger coupling with magnetic field and to increase in chemical potential. On Fig.2 intermediate case of small primary anisotropy is presented.

On Fig.4 temperature as a function of z_h , μ and c_B is presented. At small values temperature is rather sensitive to chemical potential and magnetic field presence

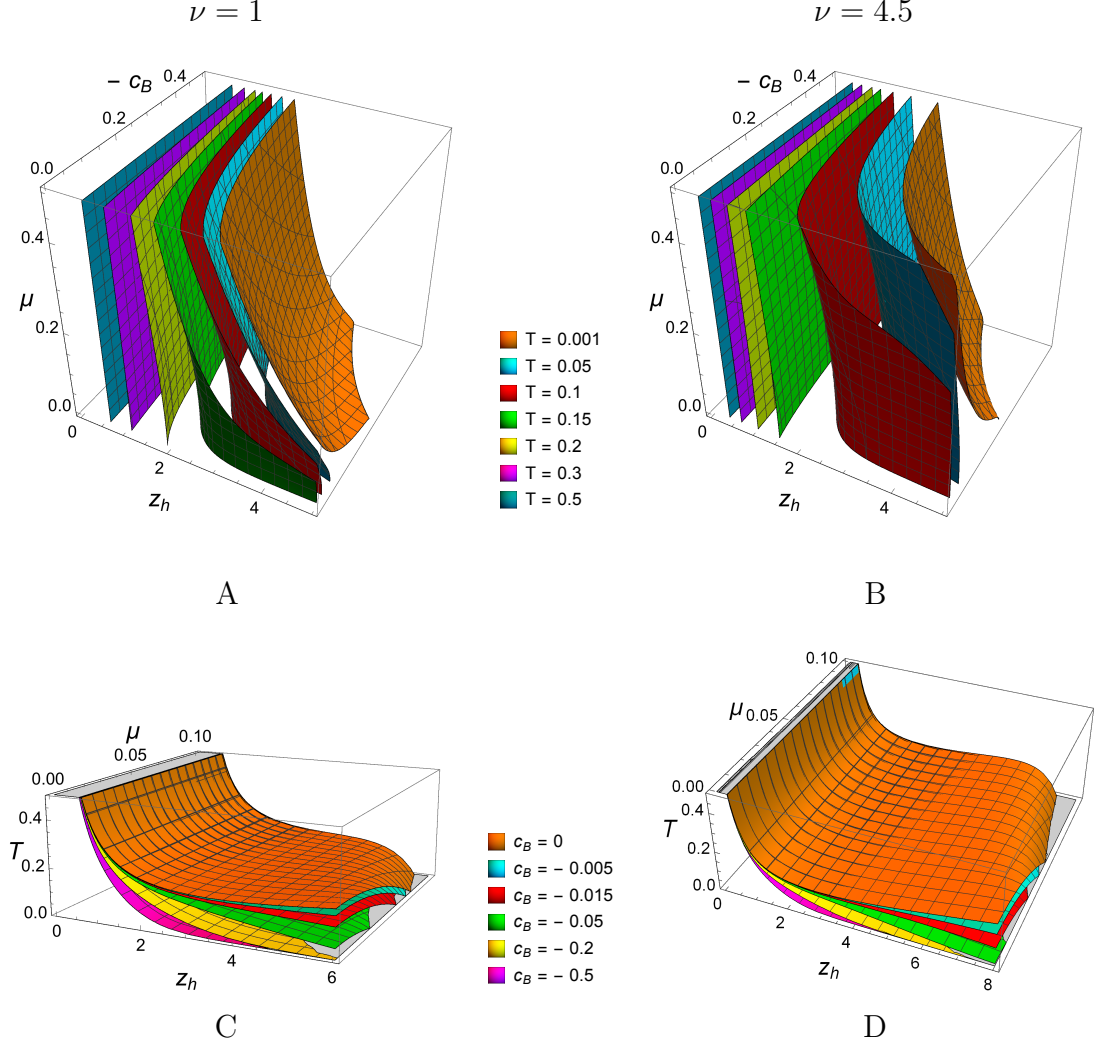


Figure 3. Contour plots of temperature depending on z_h , $-c_B$ and μ for $\nu = 1$ (A) and $\nu = 4.5$ (B). Dependence of temperature on z_h and μ for different c_B shown by different colors for $\nu = 1$ (C) $\nu = 4.5$ (D).

(Fig.4.A). The larger absolute value of μ or c_B leads to smaller z_h for the fixed temperature. But their influence significantly weakens with increasing temperature. Isotherm surfaces for large T are almost flat and parallel to $\mu - c_B$ plane, i.e. they are determined mainly by horizon, so that contribution of magnetic field and chemical potential are minor. For $\nu = 4.5$ (Fig.4.B) this process is faster than for $\nu = 1$ as influence of μ and c_B is weakened from the start.

On Fig.4C,D $T(z_h, \mu)$ for different c_B and $\nu = 1, 4.5$ is presented. Here we see the effects discussed above in relation to Fig.1, 2. Each colored surface corresponds to some c_B value, and the surfaces corresponding to larger absolute values of c_B lie below. For $\nu = 1$ (Fig.4C) surface for fixed c_B is flatter than for $\nu = 4.5$ (Fig.4D).

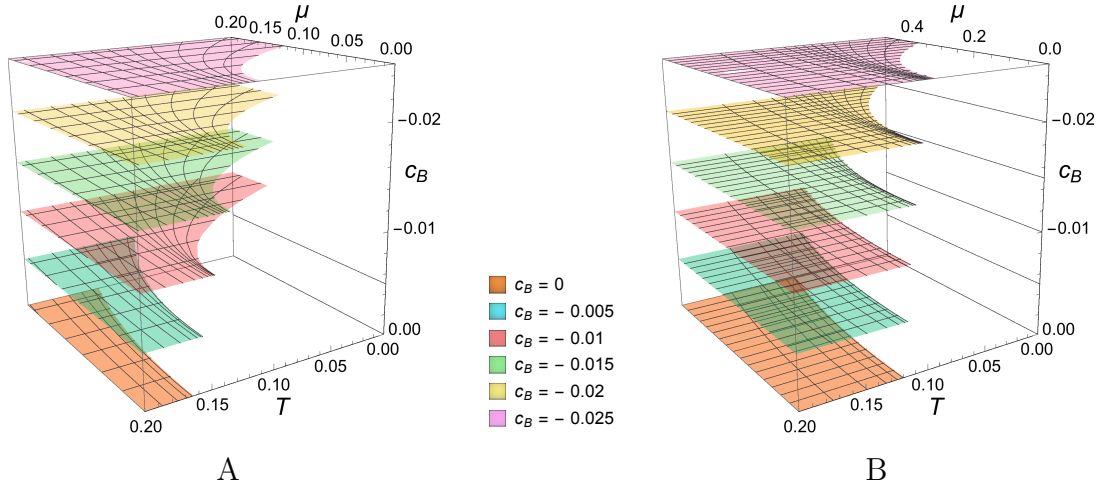


Figure 4. Domains of physical parameters of AHM (anisotropic holographic matter). Dependence of the temperature on z_h for $0 \leq \mu \leq 0.2$ and $-0.025 \leq c_B \leq 0$ for $\nu = 1$ (A) and for $\nu = 4.5$ (B). Fixed c_B values are shown by different colors.

On Fig.4 possible temperature values depending on magnetic field influence and chemical potential are shown. Planes corresponding to some fixed (descrete) values of c_B are highlighted as levels for clarity. Empty spaces mean regions with unattainable temperature values.

3 Numerical Results

The main ingredient of our calculations is a finding position of the dynamical wall for effective potentials. The effective potentials depend on the orientation. In particular cases for orientations xY_1 , xY_2 and y_1Y_2 the effective potentials are given by equations (2.49), (2.50) and (2.51). We denote the corresponding potentials as \mathcal{V}_1 , \mathcal{V}_2 and \mathcal{V}_3 for simplicity. In the next subsections we present the forms of these potentials. The effective potentials depend on c , z_0 , z_h and c_B . Note that effective potential does not depend on μ .

3.1 Wilson loop W_{xY_1}

The behavior of the effective potential \mathcal{V}_1 that corresponds to the Wilson loop W_{xY_1} on the magnetic field is presented on Fig.5.

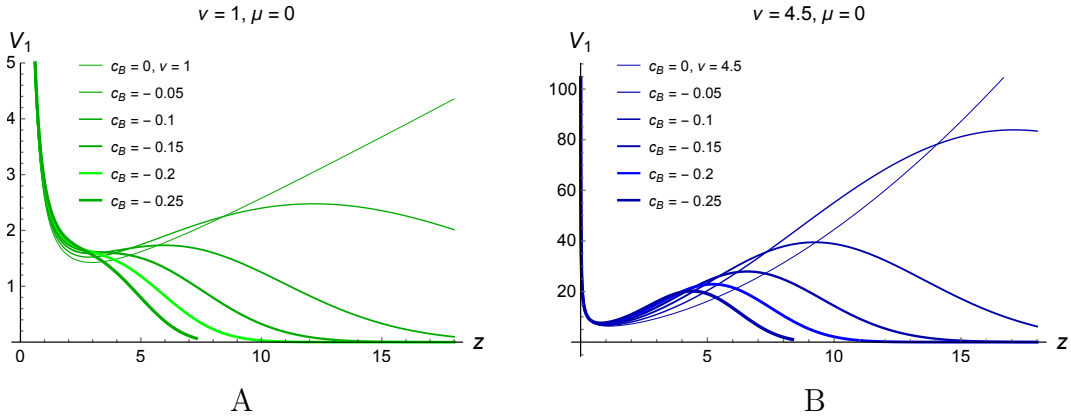


Figure 5. The dependence of the effective potential \mathcal{V}_1 on the magnetic field for $\nu = 1$ (A) and $\nu = 4.5$ (B).

We see that \mathcal{V}_1 has local minimums, i.e. has dynamical walls where $\mathcal{V}'(z) = 0$ for $0 < c_B < c_{B,cr}$. At $c_{B,cr} = 0.2$ for $\nu = 1$ the effective potential has an inflection point and for $c_B > c_{B,cr}$ the dynamical walls disappear. Locations of the dynamical walls depends on the value of c_B and are given in the Tables 1 and 2.

To get the string tension of the spatial Wilson loop we have to find the minimal value of effective potential at the dynamical wall and at the horizon. We show both values of effective potential in following plots. In Fig.6 and Fig.7 dependence of σ_1 on temperature for different values c_B and μ is presented in primary isotropic case.

\mathcal{V}_1	$\nu = 1$			
$-c_B$	0	0.05	0.1	0.138
z_{DW}	2.969	2.899	2.849	3.579

Table 1. Locations of DW for \mathcal{V}_1 at $\nu = 1$.

\mathcal{V}_1	$\nu = 4.5$						
$-c_B$	0	0.02	0.05	0.1	0.15	0.2	0.25
z_{DW}	1.131	1.083	1.031	0.952	0.896	0.841	0.798

Table 2. Locations of DW for \mathcal{V}_1 at $\nu = 4.5$.

Green lines depict the dependence of $\sigma(z_h)$ on temperature, cyan lines depict the dependence of $\sigma(z_{DW})$ on temperature. In Fig.9 and Fig.10 dependence of σ_1 on temperature for different values c_B and μ is presented in primary anisotropic case ($\nu = 4.5$). Blue lines depict the dependence of $\sigma(z_h)$ on temperature, cyan lines depict the dependence of $\sigma(z_{DW})$ on temperature. We see the phase transition between two connected string configuration with different values of string tension: $\sigma(z_{DW})$ and $\sigma(z_h)$ (see also Sect.2.2). For this phase transition the second derivative of string tension $\partial^2\sigma/\partial T^2$ undergoes a jump. In Fig.11 transparent surfaces correspond to the configurations touching the horizon, and less transparent ones to the configurations touching the dynamic wall. The phase transition corresponds to the transition from the DW configuration to the horizon configuration and is located at boundaries between light and dark surfaces. In Fig.12 locations of phase transition of σ_1 is presented for $\nu = 1$ and for $\nu = 4.5$.

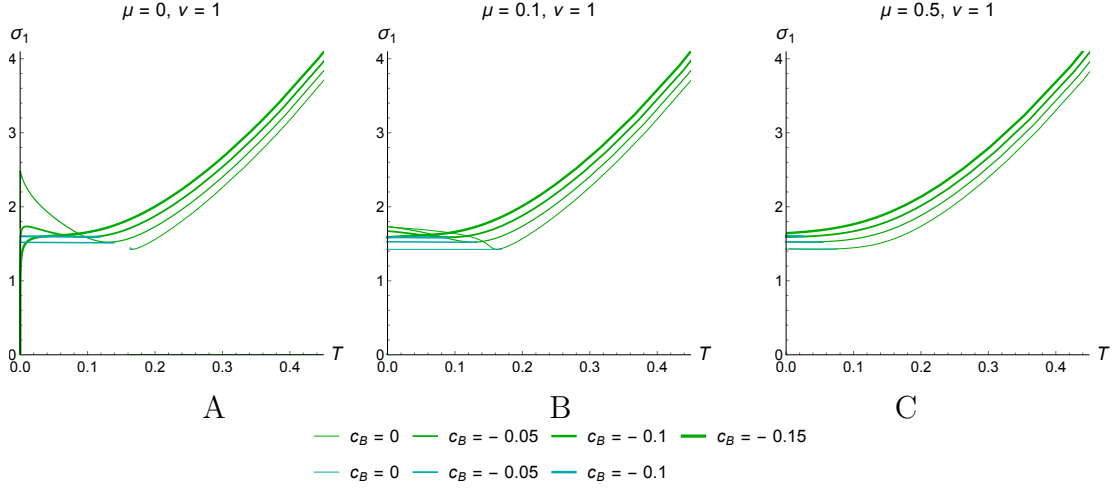


Figure 6. Dependence of σ_1 on temperature for different values of c_B for $\mu = 0$ (A), $\mu = 0.1$ (B) and $\mu = 0.5$ (C); $\nu = 1$.

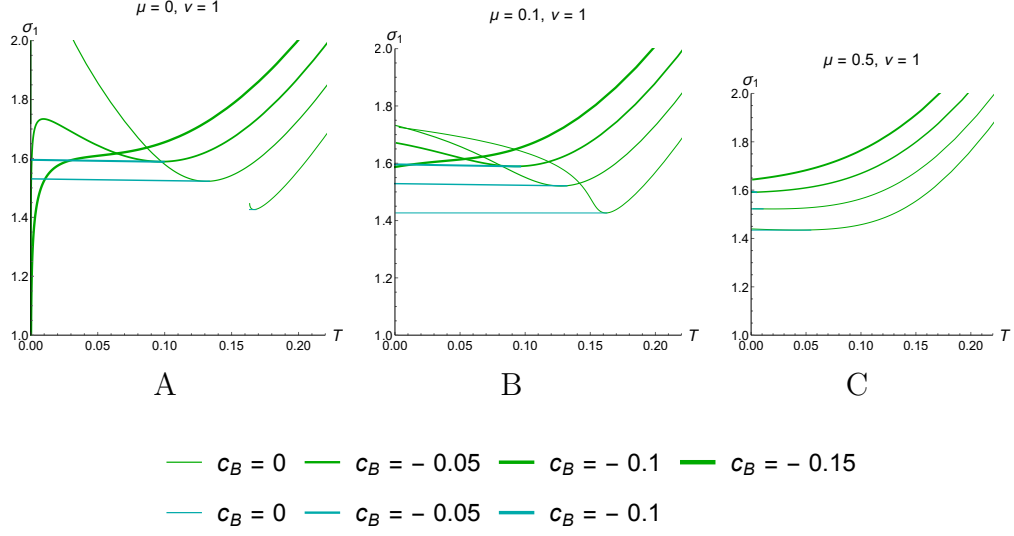


Figure 7. Dependence of σ_1 from Fig.6 in larger scale. Plot legends are the same for all plots.

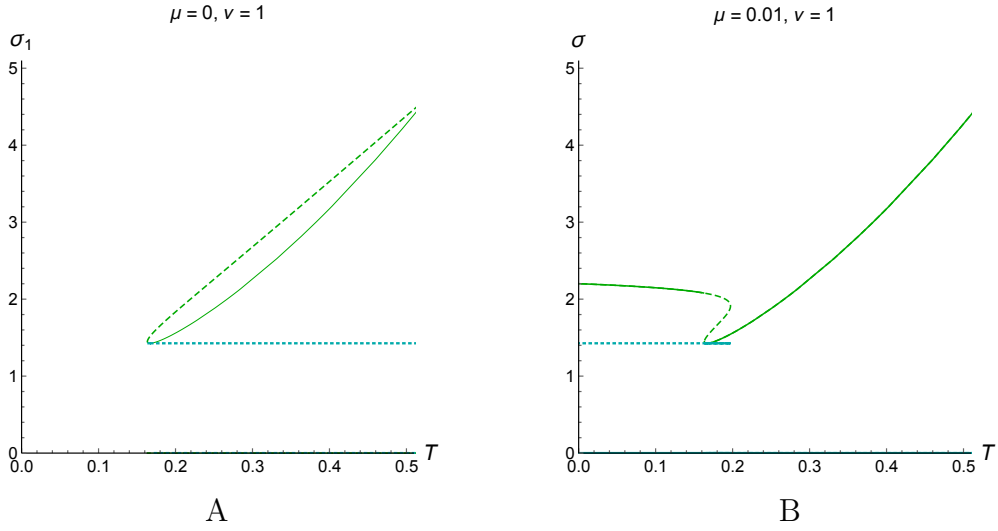


Figure 8. Phase transitions in details for $\mu = 0$ (A) and $\mu = 0.01$ (B); $c_B = 0$.

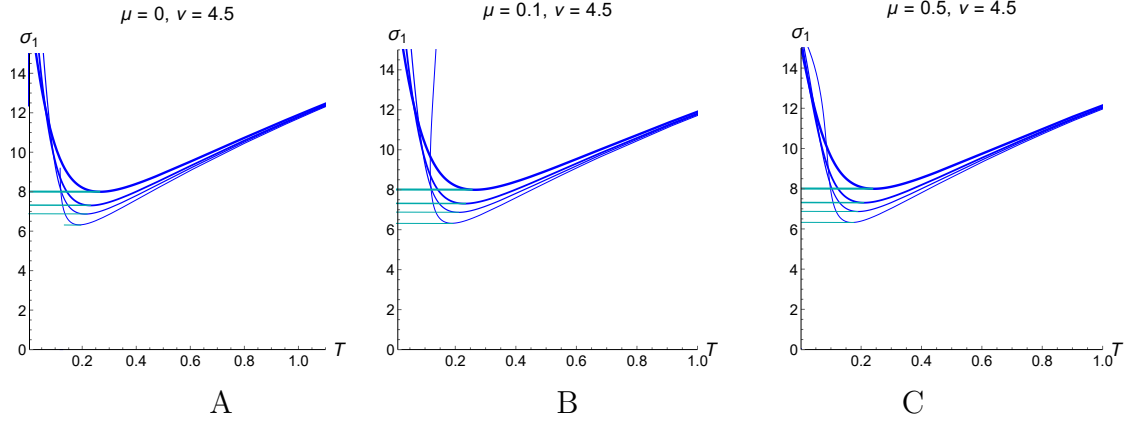


Figure 9. Dependence of σ_1 on temperature and magnetic field for $\mu = 0$ (A), $\mu = 0.1$ (B) and $\mu = 0.5$ (C); $\nu = 4.5$.

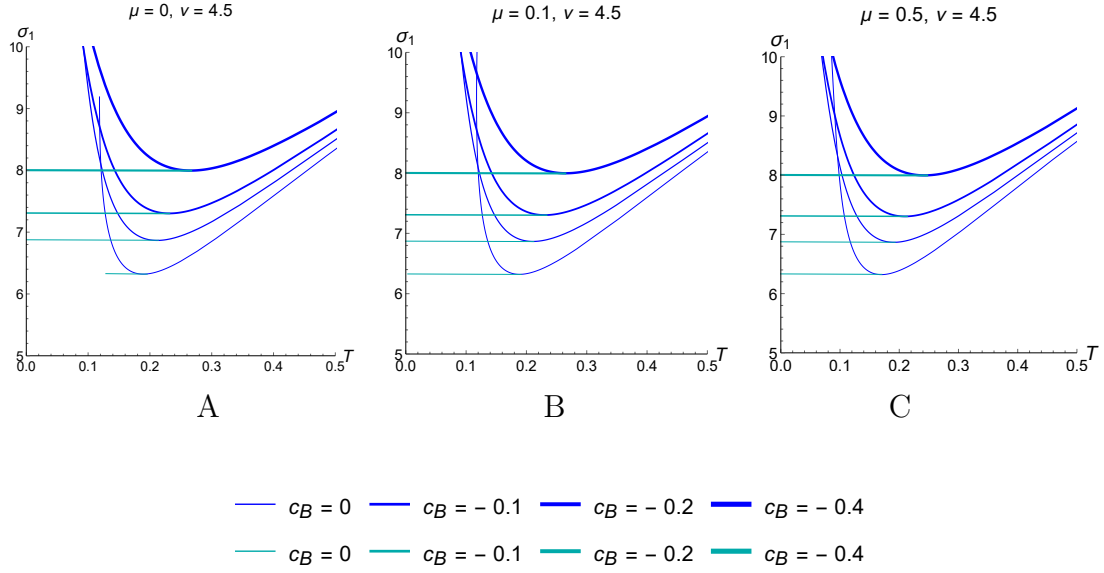


Figure 10. Dependence of σ_1 from Fig.9 in larger scale. Plot legends are the same for all plots.

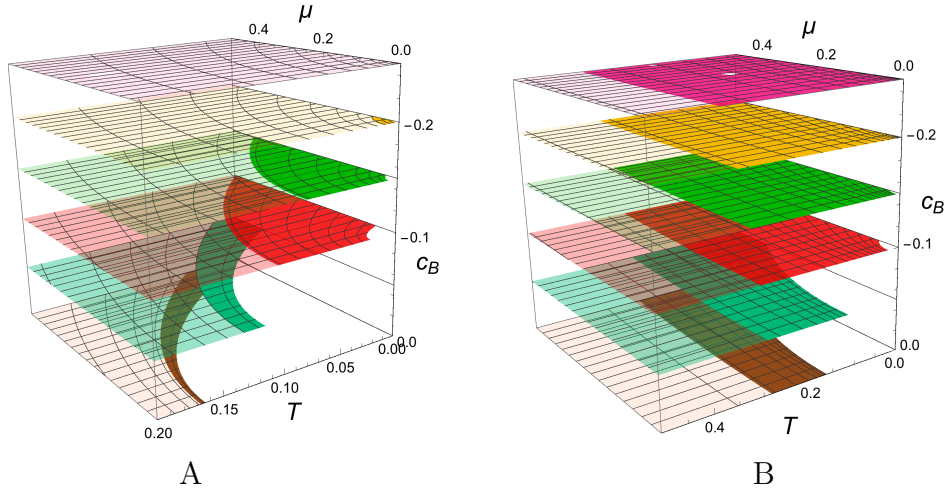


Figure 11. Transparent surfaces show the configurations touching the horizon, and less transparent ones – the configurations touching the dynamic wall for $\nu = 1$ (A) and $\nu = 4.5$ (B). The phase transition corresponds to the transition from the DW configuration to the horizon configuration and is located at boundaries between light and dark surfaces.

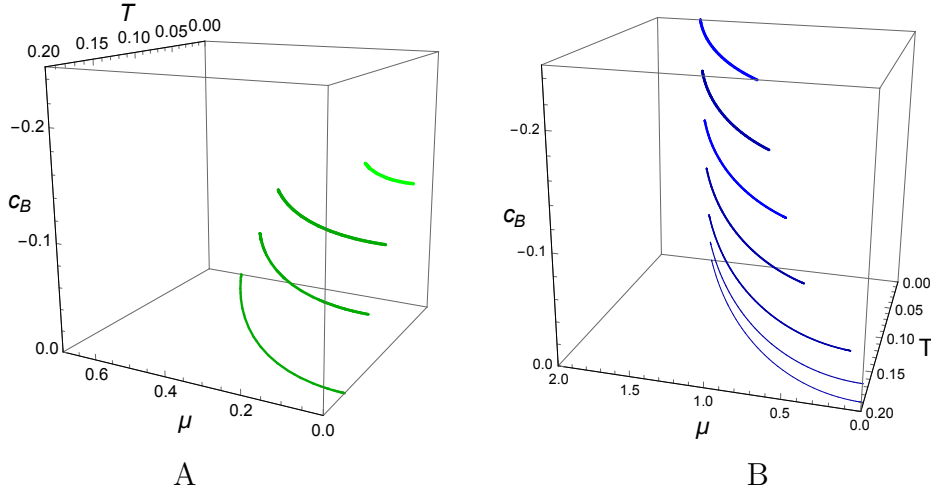


Figure 12. Locations of phase transition of σ_1 corresponding to the transition from the DW configuration to the horizon configuration for $\nu = 1$ (A) and $\nu = 4.5$ (B).

3.2 Wilson loop W_{xY_2}

In Fig.13 the effective potential \mathcal{V}_2 is presented as function of z for different c_B in primary isotopic ($\nu = 1$) and primary anisotropic ($\nu = 4.5$) cases.

In Fig.14 and Fig.15 dependence of σ_2 on temperature is presented for different values of chemical potentials μ and c_B in primary isotropic case. In Fig.16 more detailed pictures with indications of thermodynamically unstable phases are shown. In Fig.17 and Fig.18 dependence of σ_2 on temperature is presented for different values of chemical potentials μ and c_B in primary anisotropic case ($\nu = 4.5$). In both cases

we can see that there are two values of σ for some temperature values. This is the consequence of a multi-valued dependence of temperature on the size of horizon and two-valued dependence of sigma on the size of horizon for some sets of parameters c_B , ν and μ . In Fig.16 the situation with phase transitions is depicted in details for $\mu = 0$, $\mu = 0.01$, $c_B = 0$ in both cases. The result for \mathcal{V}_2 is qualitatively similar to results for \mathcal{V}_1 . Dynamic wall positions are presented in Tables 3 and 4.

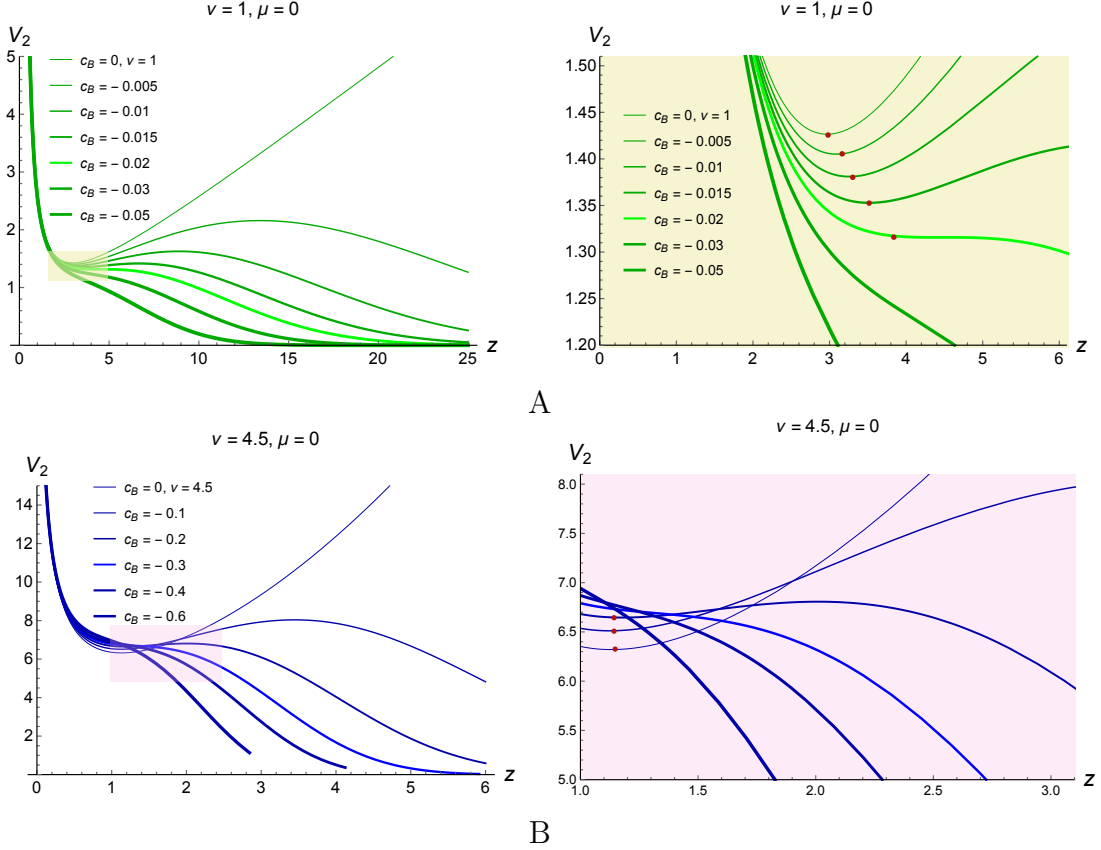


Figure 13. Effective potential \mathcal{V}_2 as function of z for different c_B ; $\nu = 1$ (A) and $\nu = 4.5$ (B). Locations of DW are indicated by dots. We see that for $\mu = 0$ at large c_B DW disappears. Here $c_{B,DWcr} \approx 0.2$ for $\nu = 1$ and $c_{B,DWcr} \approx 0.3$ for $\nu = 4.5$.

\mathcal{V}_2	$\nu = 1$			
$-c_B$	0	0.05	0.1	0.15
z_{DW}	2.952	3.110	3.238	3.465

Table 3. Locations of DW for \mathcal{V}_2 at $\nu = 1$

\mathcal{V}_2	$\nu = 4.5$						
$-c_B$	0	0.02	0.05	0.1	0.15	0.21	0.265
z_{DW}	1.130	1.126	1.124	1.124	1.142	1.178	1.192

Table 4. Locations of DW for \mathcal{V}_2 at $\nu = 4.5$

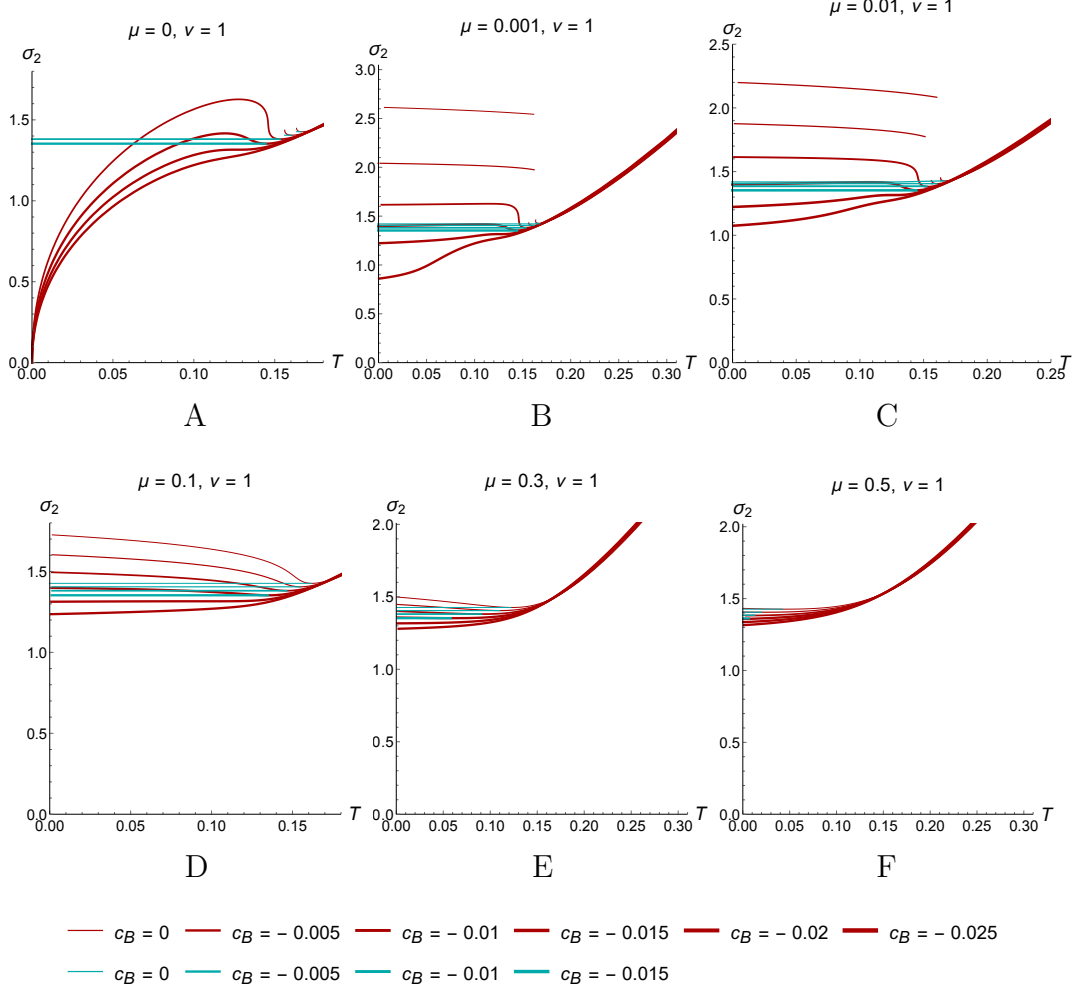


Figure 14. Dependence of σ_2 on temperature and c_B for $\mu = 0$ (A), 0.001 (B), 0.01 (C), 0.1 (D), 0.3 (E) and 0.5 (F); $\nu = 1$. Plot legends are the same for all plots.

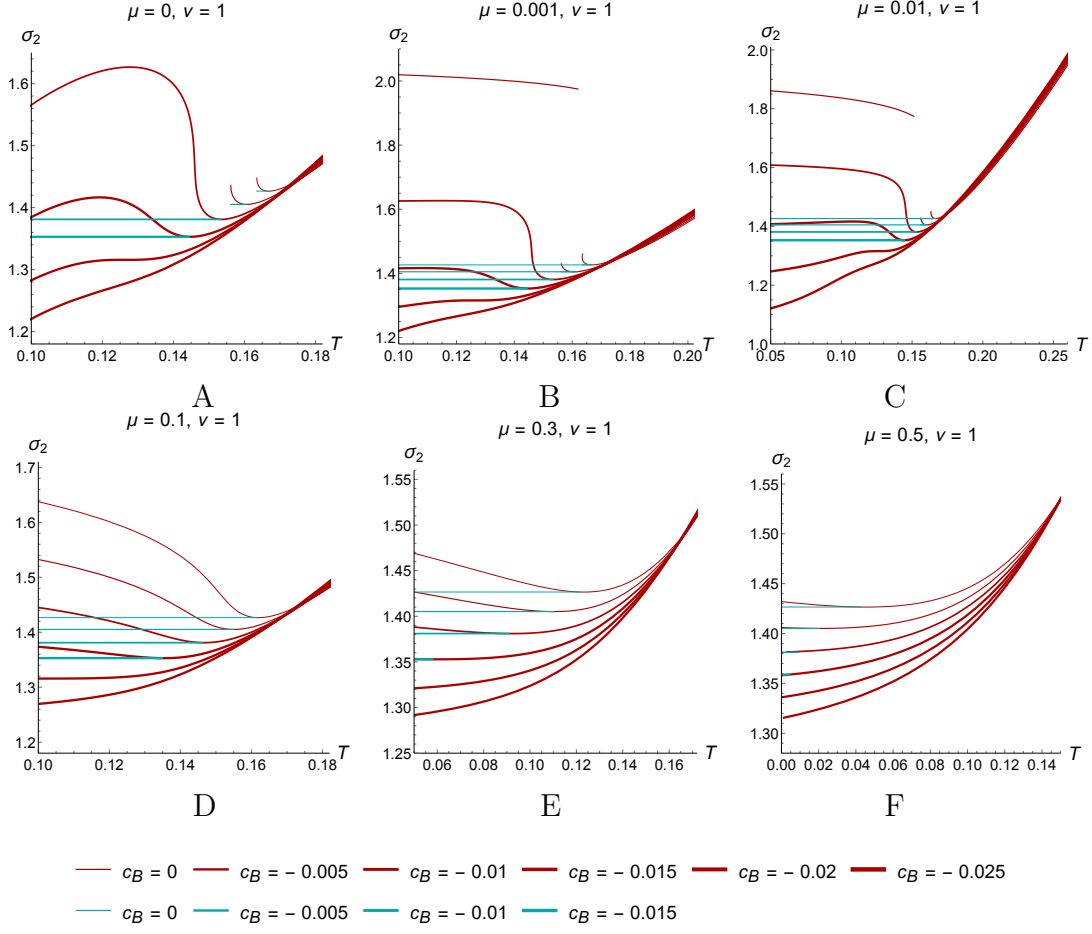


Figure 15. Dependence of σ_2 from Fig.14 in larger scale. Plot legends are the same for all plots.

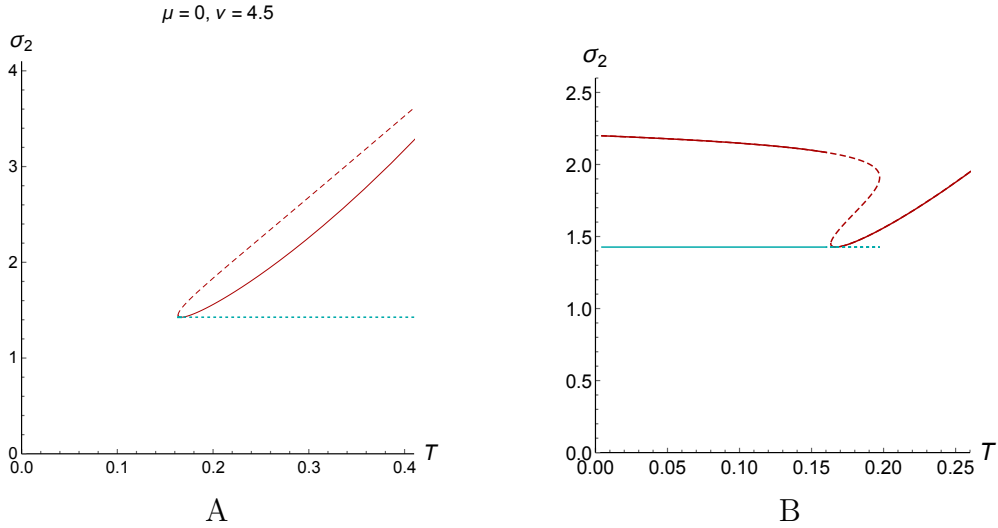


Figure 16. Phase transitions in details for $\mu = 0$ (A) and $\mu = 0.01$ (B); $c_B = 0$.

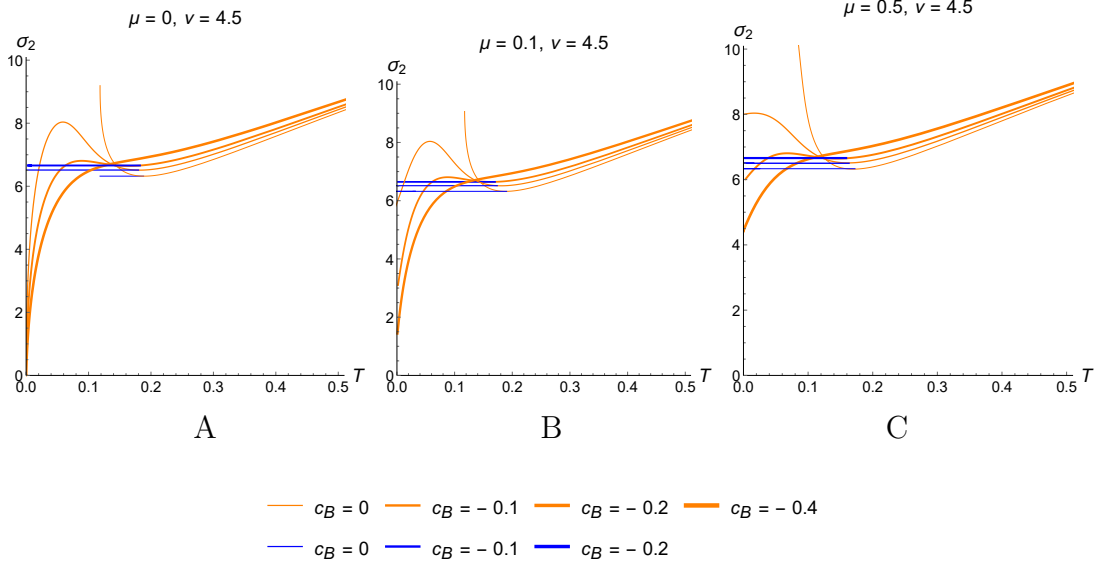


Figure 17. Dependence of σ_2 on temperature and c_B for $\mu = 0$ (A), 0.1 (B) and 0.5 (C); $\nu = 4.5$. Plot legends are the same for all plots.

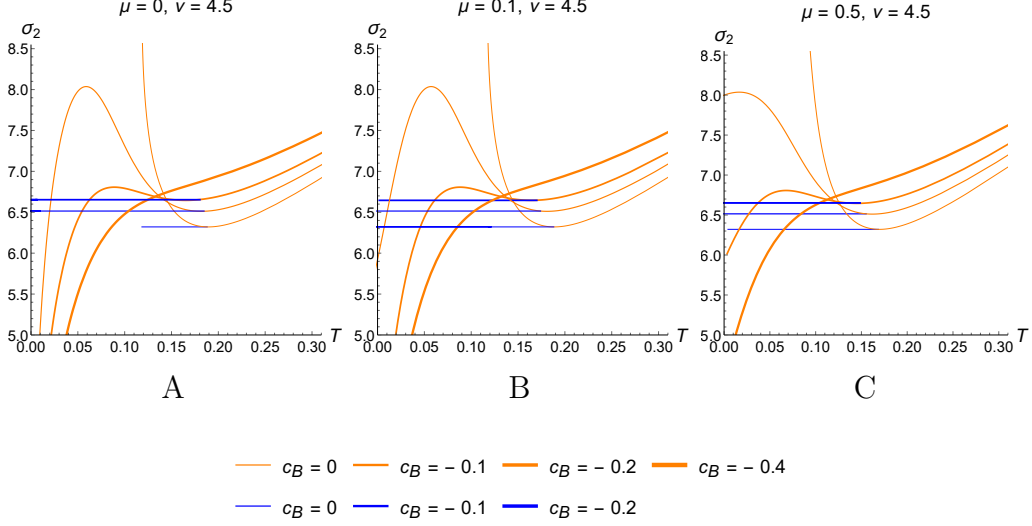


Figure 18. Dependence of σ_2 from Fig.17 in larger scale. Plot legends are the same for all plots.

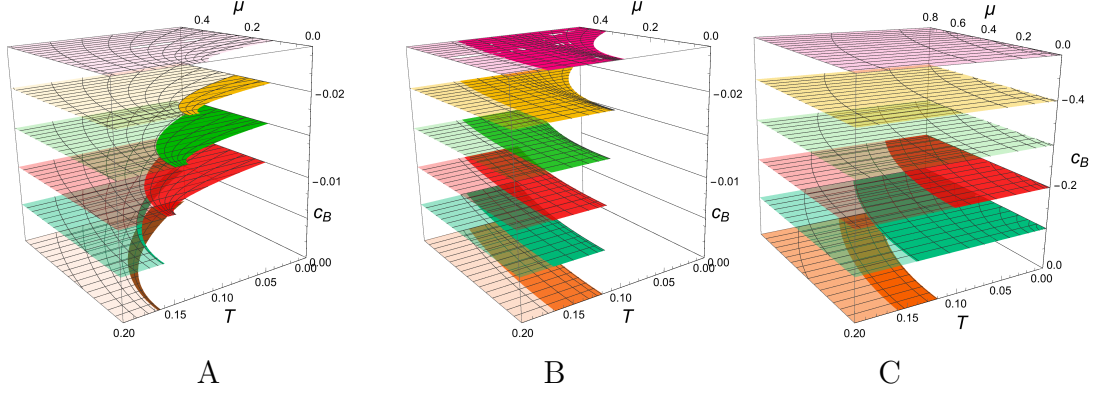


Figure 19. Phase transitions for $\nu = 1$ (A) and $\nu = 4.5$ (B,C).

Finally, we get the surfaces that depict phase transition presented at Fig.19 and Fig.20. These results can be compared with \mathcal{V}_1 consideration from previous subsection.

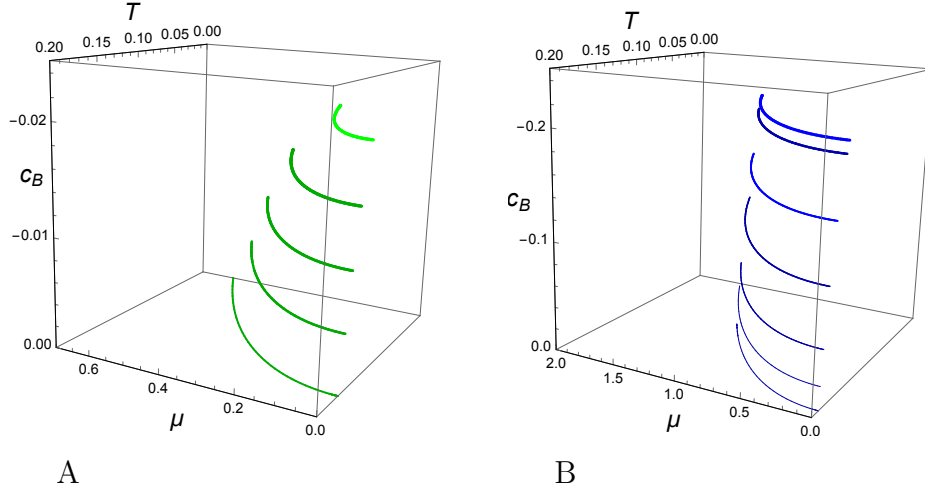


Figure 20. Phase transitions of \mathcal{V}_2 for $\nu = 1$ (A) and $\nu = 4.5$ (B). Light line represents the set of parameters where phase transitions disappear.

3.3 Wilson loop $W_{y_1 Y_2}$

In Fig.21 the effective potential dependence on z is presented. The form of the potential \mathcal{V}_3 depends on c_B and ν . The DW disappears with increasing c_B . The effective potential changes its behavior due to the dilation field asymptotic on the boundary $z = \epsilon$, so that $\mathcal{V}(0) = \infty$ for $\nu < \nu_{cr}$ and $\mathcal{V}(0) = 0$ for $\nu > \nu_{cr}$, $\nu_{cr} = 2.48$. This fact is demonstrated also in Fig.22, where the effective potential dependence on z is presented for $\nu = 2$ and $\nu = 4.5$. This behavior of the effective potential means that for large values of anisotropic parameter ν the connected string configuration disappears in the considered background.

In Fig.23.A the effective potential \mathcal{V}_3 is presented for different values of c_B and $\nu = 2$. The DW exists for all considered c_B values. In Fig.23.B σ_3 dependence on temperature T is presented. Blue lines depict the $\sigma(z_{DW})$. Dynamical wall positions for \mathcal{V}_3 are listed in Table 5.

We can also see the phase transition like it was in previous cases for \mathcal{V}_1 and \mathcal{V}_2 . In Fig.24.A the domain of acceptable physical parameters T , μ , c_B at $\nu = 2$ is depicted. In Fig.24.B phase transition is presented for $\nu = 2$ and different values of c_B . These results can be compared with \mathcal{V}_1 and \mathcal{V}_2 cases with previous subsections.

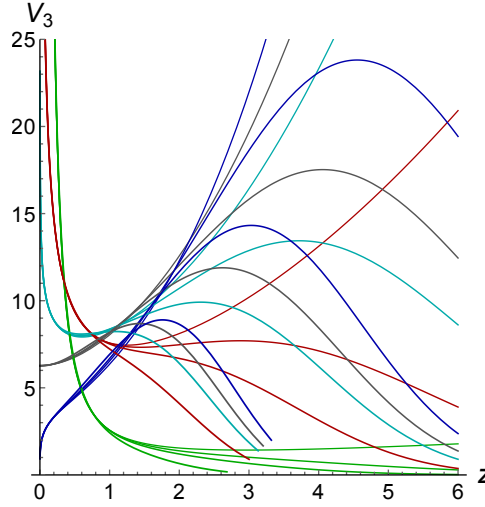


Figure 21. Effective potential \mathcal{V}_3 for $c_B = 0, 0.05, 0.1, 0.2, 0.5$ (line's thickness increases with increasing c_B) for $\nu = 1$ (green), 1.5 (red), 2 (cyan), 2.48 (gray), 4.5 (blue).

\mathcal{V}_3	$\nu = 1$		
$-c_B$	0	0.01	0.02
z_{DW}	3.030	3.352	3.978

Table 5. Locations of DW for \mathcal{V}_3 at $\nu = 1$

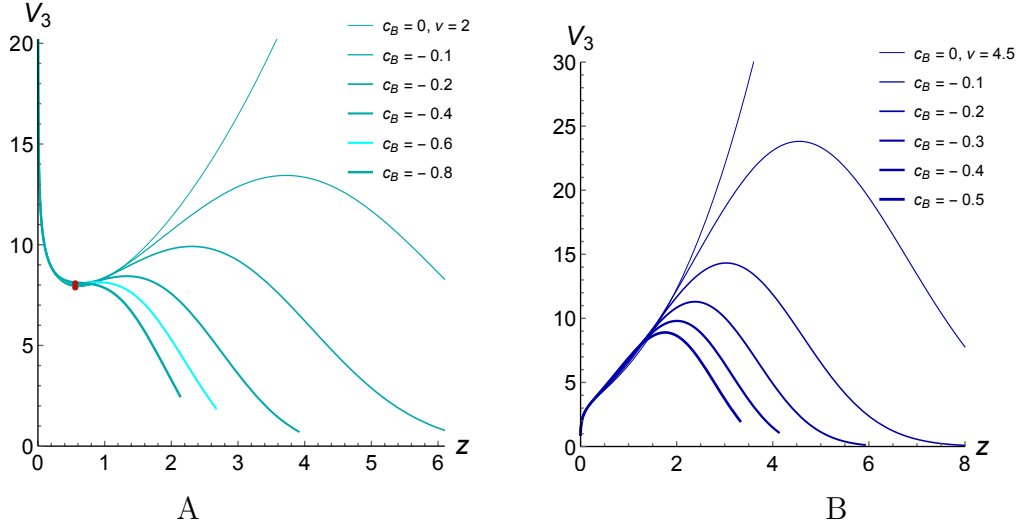


Figure 22. Effective potential \mathcal{V}_3 for different c_B values, $\nu = 2$ (A) and $\nu = 4.5$ (B).

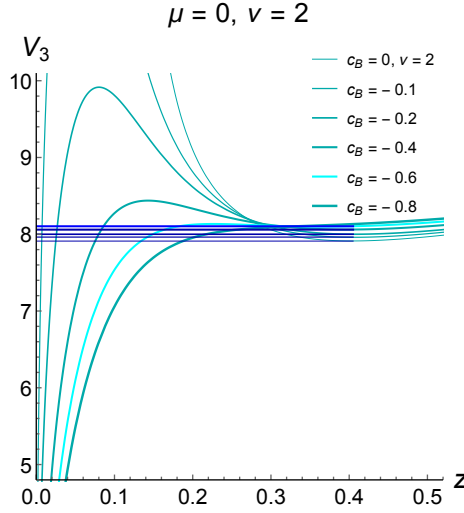


Figure 23. Dependence of σ_3 on temperature for different c_B values. Blue lines depict σ_3 calculated on the DW.

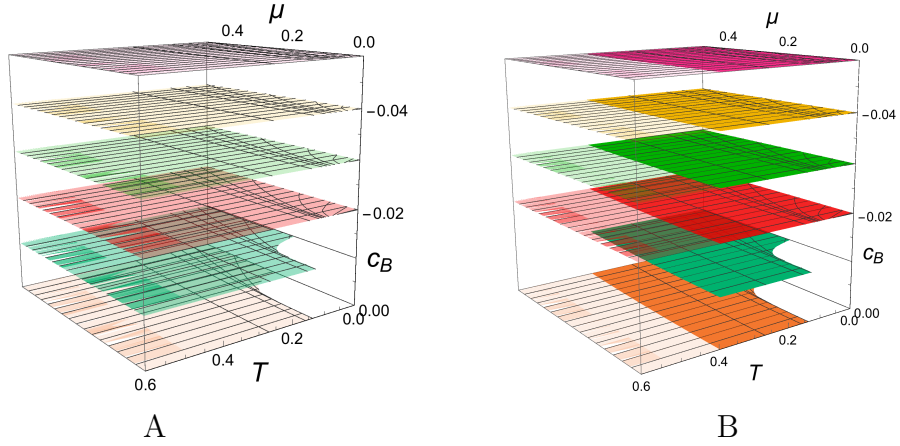


Figure 24. The domain of acceptable physical parameters T , μ , c_B ; $\nu = 2$ (A). Phase transition for σ_3 for different c_B values; $\nu = 2$ (B).

4 Conclusion

In this work expressions for the string tension σ describing differently oriented SWL in the fully anisotropic background are obtained. Dependence of σ for three particular orientations of SWL, σ_i , $i = 1, 2, 3$, on the anisotropy and external magnetic field parameters are studied. The considered orientations correspond to drag forces acting on heavy quarks moving along different directions.

Under variation of thermodynamic parameters – temperature T , chemical potential μ and magnetic field – the string tensions σ_i undergo the phase transition. Their phase transitions are related to the appearance/disappearance of dynamical walls for these effective potentials. Existence of the DW strongly depends on the parameters of anisotropy. The disappearance of DW means that we should calculate σ at the

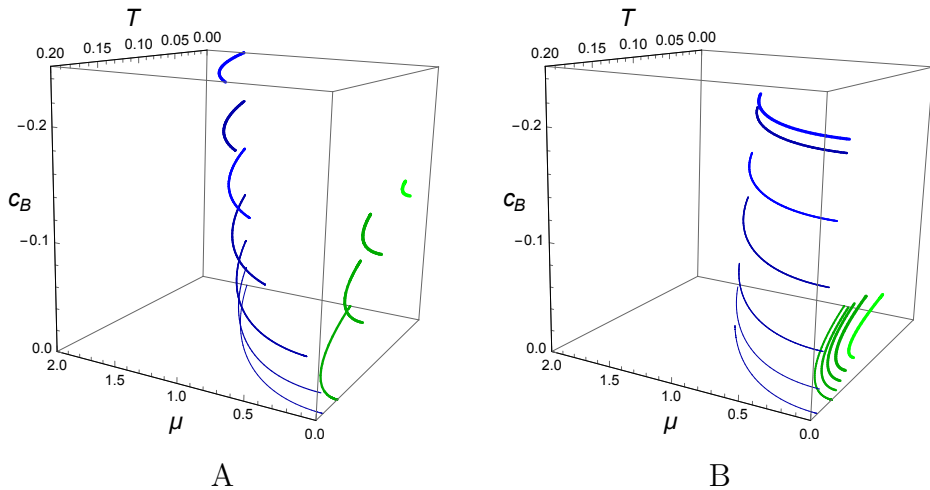


Figure 25. Phase transitions of \mathcal{V}_1 (A) and \mathcal{V}_2 (B) for $\nu = 1, 4.5$.

horizon only. In primary isotropic case, i.e. when the only source of anisotropy is the magnetic field, the DW exists for all values of z_h , so we have $\sigma(z_{DW})$ and $\sigma(z_h)$ for all z_h and the configuration with the minimal effective potential is realized. In fully anisotropic case the DW exists for $\nu < \nu_{cr}$ and $|c_B| < |c_{B,cr}|$. The DW can disappear at the point $z_{DW}(z_h, \nu, c_B)$, reached with $\nu = \nu_{cr}$, $c_B = c_{B,cr}$. Values of ν_{cr} and $c_{B,cr}$ depend on the orientation. With a slight increasing of anisotropy near $\nu = \nu_{cr}$ and $c_B = c_{B,cr}$ the DW disappears and the string tension is calculated at the horizon, therefore the phase transition between two configurations disappears too. Phase transition planes in the three dimensional space of physical parameters T, μ, c_B for σ_1 and σ_2 are presented in Fig.25 by green and blue lines for $\nu = 1$ and $\nu = 4.5$ respectively. The light green and blue lines represent to the end of the phase transitions.

It is interesting to consider SWLs and drag forces in the fully anisotropic case for different warp factors b_s , including factor corresponding light quarks, as well as the hybrid factors [58], and study the influence of the DW and anisotropy on the drag forces. Also it would be interesting to study the same problem in other anisotropic models [60, 62].

5 Acknowledgments

This work is supported by Russian Science Foundation grant №20-12-00200.

Appendix

A EOM solution

The EOM system corresponding to action (2.58) and metric (2.60) has the solution

$$A_t = \mu \frac{e^{\frac{1}{4}(c-2c_B)z^2} - e^{\frac{1}{4}(c-2c_B)z_h^2}}{1 - e^{\frac{1}{4}(c-2c_B)z_h^2}}, \quad (\text{A.1})$$

$$g = e^{c_B z^2} \left\{ 1 - \frac{\Gamma\left(1 + \frac{1}{\nu}; 0\right) - \Gamma\left(1 + \frac{1}{\nu}; \frac{3}{4}(2c_B - c)z^2\right)}{\Gamma\left(1 + \frac{1}{\nu}; 0\right) - \Gamma\left(1 + \frac{1}{\nu}; \frac{3}{4}(2c_B - c)z_h^2\right)} - \frac{\mu^2 (2c_B - c)^{-\frac{1}{\nu}}}{4L^2 \left(1 - e^{(c-2c_B)\frac{z_h^2}{4}}\right)^2} \left(\Gamma\left(1 + \frac{1}{\nu}; 0\right) - \Gamma\left(1 + \frac{1}{\nu}; \frac{3}{4}(2c_B - c)z^2\right) \right) \times \right. \\ \left. \times \left[1 - \frac{\Gamma\left(1 + \frac{1}{\nu}; 0\right) - \Gamma\left(1 + \frac{1}{\nu}; \frac{3}{4}(2c_B - c)z^2\right)}{\Gamma\left(1 + \frac{1}{\nu}; 0\right) - \Gamma\left(1 + \frac{1}{\nu}; \frac{3}{4}(2c_B - c)z_h^2\right)} \frac{\Gamma\left(1 + \frac{1}{\nu}; 0\right) - \Gamma\left(1 + \frac{1}{\nu}; (2c_B - c)z_h^2\right)}{\Gamma\left(1 + \frac{1}{\nu}; 0\right) - \Gamma\left(1 + \frac{1}{\nu}; (2c_B - c)z^2\right)} \right] \right\}, \quad (\text{A.2})$$

$$f_B = -2 \left(\frac{z}{L} \right)^{-\frac{2}{\nu}} e^{-\frac{1}{2}cz^2} \frac{c_B z}{q_B^2} g \left(\frac{3cz}{2} + \frac{2}{\nu z} - c_B z - \frac{g'}{g} \right), \quad (\text{A.3})$$

$$f_2 = 4 \left(\frac{z}{L} \right)^{2-\frac{4}{\nu}} e^{-\frac{1}{2}(c-2c_B)z^2} \frac{\nu-1}{q^2 \nu z} g \left(\frac{\nu+1}{\nu z} + \frac{3c-2c_B}{4} z - \frac{g'}{2g} \right), \quad (\text{A.4})$$

$$\phi = \frac{\sqrt{2}}{4\nu} \left\{ 2\sqrt{2} \sqrt{\nu-1} \left[\log \left(\frac{z^2}{z_0^2} \right) - \log \left(8(\nu-1) + 4\nu c_B z^2 + 3(3c-2c_B)\nu^2 z^2 + \right. \right. \right. \\ \left. \left. \left. + 2\sqrt{2} \sqrt{\nu-1} \sqrt{8(\nu-1) + 8c_B \nu z^2 + 6(3c-2c_B)\nu^2 z^2 + (3c^2 - 4c_B^2)\nu^2 z^4} \right) \right] + \right. \\ \left. + \log \left(8(\nu-1) + 4\nu c_B z_0^2 + 3(3c-2c_B)\nu^2 z_0^2 + \right. \right. \\ \left. \left. + 2\sqrt{2} \sqrt{\nu-1} \sqrt{8(\nu-1) + 8c_B \nu z_0^2 + 6(3c-2c_B)\nu^2 z_0^2 + (3c^2 - 4c_B^2)\nu^2 z_0^4} \right) \right] + \\ \left. + \sqrt{8(\nu-1) + 8c_B \nu z^2 + 6(3c-2c_B)\nu^2 z^2 + (3c^2 - 4c_B^2)\nu^2 z^4} - \right. \\ \left. - \sqrt{8(\nu-1) + 8c_B \nu z_0^2 + 6(3c-2c_B)\nu^2 z_0^2 + (3c^2 - 4c_B^2)\nu^2 z_0^4} + \right. \\ \left. + \frac{4c_B + 3(3c-2c_B)\nu}{\sqrt{3c^2 - 4c_B^2}} \times \right. \\ \left. \times \log \left(\frac{4c_B + 3(3c-2c_B)\nu z^2 \sqrt{3c^2 - 4c_B^2} \sqrt{8(\nu-1) + 8c_B \nu z^2 + 6(3c-2c_B)\nu^2 z^2 + (3c^2 - 4c_B^2)\nu^2 z^4}}{4c_B + 3(3c-2c_B)\nu^2 z_0^2 + \sqrt{3c^2 - 4c_B^2} \sqrt{8(\nu-1) + 8c_B \nu z_0^2 + 6(3c-2c_B)\nu^2 z_0^2 + (3c^2 - 4c_B^2)\nu^2 z_0^4}} \right) \right\}, \quad (\text{A.5})$$

$$V = -\frac{e^{\frac{1}{2}cz^2}}{4L^2\nu^2} \left\{ [8(1+2\nu)(1+\nu) + 2(3+2\nu)(3c-2c_B)\nu z^2 + (3c-2c_B)^2\nu^2 z^4]g - \right. \\ \left. - [2(4+5\nu) + 3(3c-2c_B)\nu z^2]g' + 2g''\nu^2 z^2 \right\}. \quad (\text{A.6})$$

Here z_0 is the point specifying the boundary condition for the dilaton field, $\phi(z_0) = 0$ [48, 58].

References

- [1] I. Y. Aref’eva, K. Rannu and P. Slepov, “Holographic Anisotropic Model for Heavy Quarks in Anisotropic Hot Dense QGP with External Magnetic Field”, [arXiv:2011.07023 [hep-th]]
- [2] J. Casalderrey-Solana, H. Liu, D. Mateos, K. Rajagopal and U. A. Wiedemann, “Gauge/String Duality, Hot QCD and Heavy Ion Collisions”, Cambridge University Press (2014) [arXiv:1101.0618 [hep-th]]
- [3] I. Ya. Aref’eva, “Holographic approach to quark-gluon plasma in heavy ion collisions”, Phys. Usp. **57**, 527 (2014)
- [4] O. DeWolfe, S. S. Gubser, C. Rosen and D. Teaney, “Heavy ions and string theory”, Prog. Part. Nucl. Phys. **75**, 86 (2014) [arXiv:1304.7794 [hep-th]]
- [5] I. Aref’eva, “Holography for Heavy Ions Collisions at LHC and NICA”, EPJ Web Conf. **164**, 01014 (2017) [arXiv:1612.08928 [hep-th]]
- [6] I. Aref’eva, “Holography for Heavy-Ion Collisions at LHC and NICA. Results of the last two years”, EPJ Web Conf. **191**, 05010 (2018)
- [7] I. Aref’eva, “Holography for Nonperturbative Study of QFT”, Phys. Part. Nucl. **51**, 489-496 (2020)
- [8] O. Andreev and V. I. Zakharov, “Heavy-quark potentials and AdS/QCD”, Phys. Rev. D **74**, 025023 (2006) [arXiv:hep-ph/0604204 [hep-ph]]
- [9] O. Andreev and V. I. Zakharov, “On Heavy-Quark Free Energies, Entropies, Polyakov Loop, and AdS/QCD”, JHEP **04**, 100 (2007) [arXiv:0611304 [hep-ph]]
- [10] U. Gursoy, E. Kiritsis, L. Mazzanti and F. Nitti, “Holography and Thermodynamics of 5D Dilaton-gravity”, JHEP **0905**, 033 (2009) [arXiv:0812.0792 [hep-th]]
- [11] U. Gursoy, E. Kiritsis, L. Mazzanti and F. Nitti, “Improved Holographic Yang-Mills at Finite Temperature: Comparison with Data”, Nucl. Phys. B **820**, 148-177 (2009) [arXiv:0903.2859 [hep-th]]
- [12] S. He, M. Huang and Q. S. Yan, “Logarithmic correction in the deformed AdS_5 model to produce the heavy quark potential and QCD beta function”, Phys. Rev. D **83**, 045034 (2011) [arXiv:1004.1880 [hep-ph]]

- [13] M. Mia, K. Dasgupta, C. Gale and S. Jeon, “Heavy Quarkonium Melting in Large N Thermal QCD”, *Phys. Lett. B* **694**, 460-466 (2011) [arXiv:1006.0055 [hep-th]]
- [14] U. Gursoy, E. Kiritsis, L. Mazzanti, G. Michalogiorgakis and F. Nitti, “Improved Holographic QCD”, *Lect. Notes Phys.* **828**, 79-146 (2011) [arXiv:1006.5461 [hep-th]]
- [15] P. Colangelo, F. Giannuzzi, S. Nicotri and V. Tangorra, “Temperature and quark density effects on the chiral condensate: An AdS/QCD study”, *Eur. Phys. J. C* **72**, 2096 (2012) [arXiv:1112.4402 [hep-ph]]
- [16] R. G. Cai, S. He and D. Li, “A hQCD model and its phase diagram in Einstein-Maxwell-Dilaton system”, *JHEP* **03**, 033 (2012) [arXiv:1201.0820 [hep-th]]
- [17] D. Giataganas, “Probing strongly coupled anisotropic plasma”, *JHEP* **07**, 031 (2012) [arXiv:1202.4436 [hep-th]]
- [18] D. Li, M. Huang and Q. S. Yan, “A dynamical soft-wall holographic QCD model for chiral symmetry breaking and linear confinement”, *Eur. Phys. J. C* **73**, 2615 (2013) [arXiv:1206.2824 [hep-th]]
- [19] S. He, S. Y. Wu, Y. Yang and P. H. Yuan, “Phase Structure in a Dynamical Soft-Wall Holographic QCD Model”, *JHEP* **04**, 093 (2013) [arXiv:1301.0385 [hep-th]]
- [20] D. Li and M. Huang, “Dynamical holographic QCD model for glueball and light meson spectra”, *JHEP* **11**, 088 (2013) [arXiv:1303.6929 [hep-ph]]
- [21] Y. Yang and P. H. Yuan, “A Refined Holographic QCD Model and QCD Phase Structure”, *JHEP* **11**, 149 (2014) [arXiv:1406.1865 [hep-th]]
- [22] I. Y. Aref’eva and A. A. Golubtsova, “Shock waves in Lifshitz-like spacetimes”, *JHEP* **04**, 011 (2015) [arXiv:1410.4595 [hep-th]]
- [23] D. Li, S. He and M. Huang, “Temperature dependent transport coefficients in a dynamical holographic QCD model”, *JHEP* **06**, 046 (2015) [arXiv:1411.5332 [hep-ph]]
- [24] R. Rougemont, R. Critelli and J. Noronha, “Holographic calculation of the QCD crossover temperature in a magnetic field”, *Phys. Rev. D* **93**, 045013 (2015) [arXiv:1505.07894 [hep-ph]]
- [25] Y. Yang and P. H. Yuan, “Confinement-deconfinement phase transition for heavy quarks in a soft wall holographic QCD model”, *JHEP* **12**, 161 (2015) [arXiv:1506.05930 [hep-th]]
- [26] K. Chelabi, Z. Fang, M. Huang, D. Li and Y. L. Wu, “Realization of chiral symmetry breaking and restoration in holographic QCD”, *Phys. Rev. D* **93**, 101901 (2016) [arXiv:1511.02721 [hep-ph]]
- [27] Z. Fang, S. He and D. Li, “Chiral and Deconfining Phase Transitions from Holographic QCD Study”, *Nucl. Phys. B* **907**, 187-207 (2016) [arXiv:1512.04062 [hep-ph]]

- [28] K. Chelabi, Z. Fang, M. Huang, D. Li and Y. L. Wu, “Chiral Phase Transition in the Soft-Wall Model of AdS/QCD”, JHEP **04**, 036 (2016) [arXiv:1512.06493 [hep-ph]]
- [29] D. S. Ageev, I. Y. Aref’eva, A. A. Golubtsova and E. Gourgoulhon, “Thermalization of holographic Wilson loops in spacetimes with spatial anisotropy”, Nucl. Phys. B **931**, 506-536 (2018) [arXiv:1606.03995 [hep-th]]
- [30] D. Li, M. Huang, Y. Yang and P. H. Yuan, “Inverse Magnetic Catalysis in the Soft-Wall Model of AdS/QCD”, JHEP **02**, 030 (2017) [arXiv:1610.04618 [hep-th]]
- [31] D. Li and M. Huang, “Chiral phase transition of QCD with $N_f = 2 + 1$ flavors from holography”, JHEP **02**, 042 (2017) [arXiv:1610.09814 [hep-ph]]
- [32] U. Gursoy, I. Iatrakis, M. Jarvinen and G. Nijs, “Inverse Magnetic Catalysis from improved Holographic QCD in the Veneziano limit”, JHEP **03**, 053 (2017) [arXiv:1611.06339 [hep-th]]
- [33] D. Dudal and S. Mahapatra, “Confining gauge theories and holographic entanglement entropy with a magnetic field”, JHEP **04**, 031 (2017) [arXiv:1612.06248 [hep-th]]
- [34] M.-W. Li, Y. Yang, P.-H. Yuan, “Approaching Confinement Structure for Light Quarks in a Holographic Soft Wall QCD Model”, Phys. Rev. D **96**, 066013 (2017) [arXiv:1703.09184 [hep-th]]
- [35] Y. Yang and P. H. Yuan, “Universal Behaviors of Speed of Sound from Holography”, Phys. Rev. D **97**, 126009 (2018) [arXiv:1705.07587 [hep-th]]
- [36] U. Gursoy, M. Jarvinen and G. Nijs, “Holographic QCD in the Veneziano limit at finite Magnetic Field and Chemical Potential”, Phys. Rev. Lett. **120**, 242002 (2018) [arXiv:1707.00872 [hep-th]]
- [37] D. Giataganas, U. Gürsoy and J. F. Pedraza, “Strongly-coupled anisotropic gauge theories and holography,” Phys. Rev. Lett. **121**, 121601 (2018) [arXiv:1708.05691 [hep-th]]
- [38] K. B. Fadafan and R. Morad, “Jets in a strongly coupled anisotropic plasma”, Eur. Phys. J. C **78**, 16 (2018) [arXiv:1710.06417 [hep-th]]
- [39] I. Ya. Aref’eva and K. A. Rannu, “Holographic Anisotropic Background with Confinement-Deconfinement Phase Transition”, JHEP **05**, 206 (2018) [arXiv:1802.05652 [hep-th]]
- [40] I. Y. Aref’eva, A. A. Golubtsova and G. Policastro, “Exact holographic RG flows and the $A_1 \times A_1$ Toda chain”, JHEP **05**, 117 (2019) [arXiv:1803.06764 [hep-th]]
- [41] I. Aref’eva, K. Rannu and P. Slepov, “Orientation Dependence of Confinement-Deconfinement Phase Transition in Anisotropic Media”, Phys. Lett. B **792**, 470-475 (2019) [arXiv:1808.05596 [hep-th]]
- [42] Z. Fang, Y. L. Wu and L. Zhang, “Chiral phase transition and QCD phase diagram from AdS/QCD”, Phys. Rev. D **99** 034028 (2019) [arXiv:1810.12525 [hep-ph]]

- [43] Jianwei Chen, Song He, Mei Huang, Danning Li, “Critical exponents of finite temperature chiral phase transition in soft-wall AdS/QCD models”, JHEP **01**, 165 (2019) [arXiv:1810.07019 [hep-ph]]
- [44] U. Gursoy, M. Jarvinen, G. Nijs and J. F. Pedraza, “Inverse Anisotropic Catalysis in Holographic QCD”, Phys. Rev. Lett. **04**, 071 (2019) [arXiv:1811.11724 [hep-th]]
- [45] A. A. Golubtsova and V. H. Nguyen, “Wilson Loops in Exact Holographic RG Flows at Zero and Finite Temperatures”, Theor. Math. Phys. **202**, 214-230 (2020) [arXiv:1906.12316 [hep-th]]
- [46] H. Bohra, D. Dudal, A. Hajilou and S. Mahapatra, “Anisotropic string tensions and inversely magnetic catalyzed deconfinement from a dynamical AdS/QCD model”, Phys. Lett. B **801**, 135184 (2020) [arXiv:1907.01852 [hep-th]]
- [47] X. Chen, D. Li, D. Hou and M. Huang, “Quarkyonic phase from quenched dynamical holographic QCD model”, JHEP **03**, 073 (2020) [arXiv:1908.02000 [hep-ph]]
- [48] I. Aref’eva, K. Rannu and P. Slepov, “Cornell potential for anisotropic QGP with non-zero chemical potential”, EPJ Web Conf. **222**, 03023 (2019)
- [49] P. Slepov, “Entanglement entropy in strongly correlated systems with confinement/deconfinement phase transition and anisotropy,” EPJ Web Conf. **222**, 03024 (2019)
- [50] Z. Fang and Y. L. Wu, “Equation of state and chiral transition in soft-wall AdS/QCD with more realistic gravitational background”, [arXiv:1909.06917 [hep-ph]]
- [51] Z. Fang and L. Zhang, “Chiral transition and meson melting with finite chemical potential in an improved soft-wall AdS/QCD Model”, [arXiv:1910.02269 [hep-ph]]
- [52] A. Ballon-Bayona and L. A. H. Mamani, “Nonlinear realization of chiral symmetry breaking in holographic soft wall models”, Phys. Rev. D **102**, 026013 (2020) [arXiv:2002.00075 [hep-ph]]
- [53] I. Y. Aref’eva, A. Patrushev and P. Slepov, “Holographic entanglement entropy in anisotropic background with confinement-deconfinement phase transition”, JHEP **07**, 043 (2020) [arXiv:2003.05847 [hep-th]]
- [54] S. He, Y. Yang and P. H. Yuan, “Analytic Study of Magnetic Catalysis in Holographic QCD”, [arXiv:2004.01965 [hep-th]]
- [55] A. Ballon-Bayona, J. P. Shock and D. Zoakos, “Magnetic catalysis and the chiral condensate in holographic QCD”, [arXiv:2005.00500 [hep-th]]
- [56] A. Ballon-Bayona, H. Boschi-Filho, E. Folco Capossoli and D. M. Rodrigues, “Criticality from EMD holography at finite temperature and density”, [arXiv:2006.08810 [hep-th]]
- [57] P. Colangelo, F. De Fazio and N. Losacco, “Chaos in a $Q\bar{Q}$ system at finite temperature and baryon density”, Phys. Rev. D **102**, 074016 (2020) [arXiv:2007.06980 [hep-ph]]

- [58] I. Y. Aref’eva, K. Rannu and P. Slepov, “Holographic Anisotropic Model for Light Quarks with Confinement-Deconfinement Phase Transition”, [arXiv:2009.05562 [hep-th]]
- [59] M. W. Li, Y. Yang and P. H. Yuan, “Analytic Study on Chiral Phase Transition in Holographic QCD”, [arXiv:2009.05694 [hep-th]]
- [60] H. Bohra, D. Dudal, A. Hajilou and S. Mahapatra, “Chiral transition in the probe approximation from an Einstein-Maxwell-dilaton gravity model”, [arXiv:2010.04578 [hep-th]]
- [61] D. M. Rodrigues, D. Li, E. Folco Capossoli and H. Boschi-Filho, “Finite density effects on chiral symmetry breaking in a magnetic field in 2+1 dimensions from holography”, [arXiv:2010.06762 [hep-th]]
- [62] U. Gürsoy, M. Järvinen, G. Nijs and J. F. Pedraza, “On the interplay between magnetic field and anisotropy in holographic QCD,” [arXiv:2011.09474 [hep-th]].
- [63] F. R. Brown, F. P. Butler, H. Chen, N. H. Christ, Z. h. Dong, W. Schaffer, L. I. Unger and A. Vaccarino, “On the existence of a phase transition for QCD with three light quarks”, Phys. Rev. Lett. **65**, 2491-2494 (1990)
- [64] O. Philipsen, PoS **LATTICE2019**, 273 (2019) [arXiv:1912.04827 [hep-lat]]
- [65] S. J. Sin and I. Zahed, “Ampere’s Law and Energy Loss in AdS/CFT Duality”, Phys. Lett. B **648**, 318 (2007) [arXiv:0606049 [hep-th]]
- [66] O. Andreev, “Drag Force on Heavy Quarks and Spatial String Tension”, Mod. Phys. Lett. A **33**, 1850041 (2018) [arXiv: 1707.05045[hep-ph]]
- [67] C. Herzog, A. Karch, P. Kovtun, C. Kozcaz, and L. Yaffe, “Energy loss of a heavy quark moving through $N = 4$ supersymmetric Yang-Mills plasma”, JHEP **07** 013 (2006) [arXiv:0605158 [hep-th]]
- [68] S. S. Gubser, “Drag force in AdS/CFT”, Phys. Rev. D **74**, 126005 (2006) [arXiv:0605182 [hep-th]]
- [69] J. Casalderrey-Solana and D. Teaney, “Heavy quark diffusion in strongly coupled $N = 4$ Yang-Mills”, Phys. Rev. D **74**, 085012 (2006) [arXiv:0605199 [hep-ph]]
- [70] S. S. Gubser, “Comparing the drag force on heavy quarks in $N = 4$ super-Yang-Mills theory and QCD”, Phys. Rev. D **76** 126003 (2007) [arXiv:0611272 [hep-th]]
- [71] U. Gursoy, E. Kiritsis, G. Michalogiorgakis and F. Nitti, “Thermal transport and drag force in improved holographic QCD”, JHEP **12**, 56 (2009) [arXiv:0906.1890 [hep-th]]
- [72] M. Chernicoff, D. Fernandez, D. Mateos and D. Trancanelli, “Drag force in a strongly coupled anisotropic plasma”, JHEP **1208**, 100 (2012), [arXiv:1202.3696 [hep-th]]
- [73] D. Giataganas and H. Soltanpanahi, “Heavy quark diffusion in strongly coupled anisotropic plasmas”, JHEP **06**, 47 (2014) [arXiv:1312.7474 [hep-th]]

- [74] S. Chakraborty and N. Haque, “Drag force in strongly coupled, anisotropic plasma at finite chemical potential”, JHEP **12**, 175 (2014) [arXiv:1410.7040 [hep-th]]
- [75] L. Cheng, X. H. Ge and S. Y. Wu, “Drag force of anisotropic plasma at finite $U(1)$ chemical potential”, Eur. Phys. J. C **76**, 256 (2016) [arXiv:1412.8433 [hep-th]]
- [76] K. Rajagopal and A. V. Sadofyev, “Chiral drag force”, JHEP **10**, 18 (2015) [arXiv:1505.07379 [hep-th]]
- [77] K. A. Mamo, “Energy loss of a nonaccelerating quark moving through a strongly coupled $N = 4$ super Yang-Mills vacuum or plasma in strong magnetic field”, Phys. Rev. D **94**, 041901 (2016) [arXiv:1606.01598 [hep-th]]
- [78] R. Rougemont, A. Ficnar, S. Finazzo and J. Noronha, “Energy loss, equilibration, and thermodynamics of a baryon rich strongly coupled quark-gluon plasma”, JHEP **1604**, 102 (2016) [arXiv:1507.06556 [hep-th]]
- [79] S. I. Finazzo, R. Critelli, R. Rougemont and J. Noronha, “Momentum transport in strongly coupled anisotropic plasmas in the presence of strong magnetic fields”, Phys. Rev. D **94**, 054020 (2016) Erratum: [Phys. Rev. D **96**, 019903 (2017)] [arXiv:1605.06061 [hep-ph]]
- [80] E. Brehm, “Heavy Quarks in Strongly Coupled Non-Conformal Plasmas with Anisotropy”, JHEP **06**, 128 (2019) arXiv:1711.08943 [hep-th]
- [81] Z. R. Zhu, S. Q. Feng, Y. F. Shi and Y. Zhong, “Energy loss of heavy and light quarks in holographic magnetized background”, Phys. Rev. D **99**, 126001 (2019) [arXiv:1901.09304 [hep-ph]]
- [82] Z. q. Zhang, “Light quark energy loss in strongly coupled $N=4$ SYM plasma with magnetic field,” Phys. Lett. B **793**, 308-312 (2019)